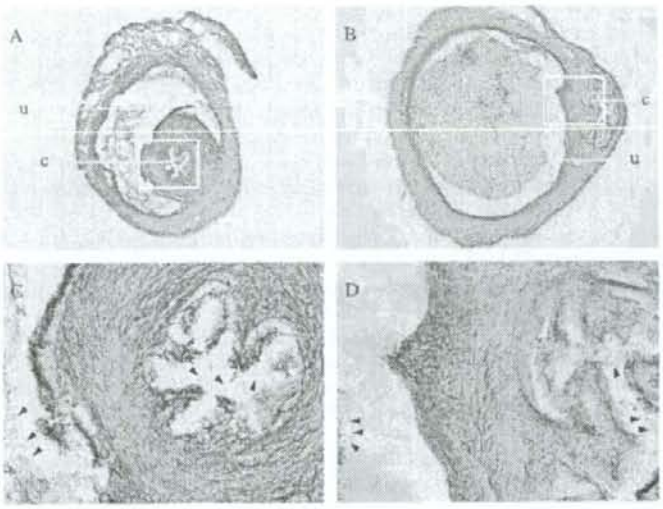

Figure 7 Migration of *Cd52*$^{+/-}$ sperm into oviduct. Sperm transits from uterus to oviduct were observed by removing the uterotubal junction 2 h after coitus and making frozen sections stained with hematoxylin. (A, C) heterozygous type: (B, D) *Cd52*$^{-/-}$. Boxed areas in (A) and (B) were magnified in (C) and (D). Arrow heads indicate sperm present in the uterus (u) and colliculus (c).

Table 2 Comparison of fertilizing ability of sperm prepared from CD52 +/+, +/− and −/− mice *in vitro*

CD52	Total number of eggs examined	8 h after insemination: Number of pronuclear eggs ($n = 3$)*	24 h after insemination: Number of 2-cell eggs (%) ($n = 3$)
+/+	195	188 (96.4 ± 2.6)	180 (92.3 ± 2.5)
+/−	273	262 (96.0 ± 2.6)	252 (92.3 ± 5.2)
−/−	229	218 (95.2 ± 2.6)	216 (94.3 ± 1.2)

*Polyspermy eggs with more than three pronuclei were eliminated from the count.
Mean ± SD of three independent IVF results using three different males.

Table 3 Fertilized eggs recovered from oviducts from copulated females

Male genotype	Number of females used	Total number of eggs obtained	Fertilized eggs*	Fertilization (%) mean ± SD
+/+ or +/−	7	277	256	94.9 ± 2.8
−/−	7	235	222	95.2 ± 5.4

*Assessed by observing the pronuclear formation.

CD52 is a GPI-anchored membrane protein found in mouse, rat, monkey, dog and human (Hale 2001). Although the lengths of the mature peptides are different among species, all of them have a single potential site for the N-linked glycosylation. The rat CD52 antigen has been characterized for many years as the "major maturation-associated antigen" of sperm (Kirchhoff 1996; Yeung *et al.* 2001). It is the most abundant antigen among the sperm glycoproteins and its acquisition during epididymal transit explains much of the remarkable change in surface charge and lectin-binding characteristics which occurs during sperm maturation (Kirchhoff & Schroter 2001). In view of the accumulation of CD52 in rat and human sperm, it is natural to expect an important role of CD52 in sperm maturation in various species. Therefore, we chose CD52 as a candidate gene to disrupt to elucidate the mechanism of epididymal maturation process toward fertilization.

© 2008 The Authors
Journal compilation © 2008 by the Molecular Biology Society of Japan/Blackwell Publishing Ltd.

Although CD52 was highly expressed in the epididymal tissues, the disruption of CD52 caused no apparent effect on the epididymal functions *per se*. As an alternative role, we could speculate that CD52, as one of the membrane proteins after transition to sperm, is functioning to interact with the female reproductive tract. However, the sperm from *Cd52*-deficient mice could successfully migrate into the oviduct and fertilize the eggs and *Cd52*-deficient males sired similar numbers of pups. The fertilizing ability of *Cd52*-deficient males remained normal even at 50 weeks of age (data not shown), indicating that no immunological disorders in the reproductive tract took place, differing from the case of CD59-disrupted mouse line, in which a progressive loss of fertility associated with immobile dysmorphic and fewer sperm cells after 5 months of age was observed (Qin *et al.* 2003; Qin *et al.* 2005). Thus with respect to all these aspects, CD52 turned out to be not essential in the fertilization system. Approximately 25% of the sperm population had detectable CD52. If CD52 has an inhibitory or stimulatory activity on sperm function when attached to the sperm surface, the remaining CD52-free population might mask the effect of CD52 in our experimental system. Although, no apparent phenotype of CD52 disruption was observed in the present experiment, the fact that the CD52 has been retained as an active gene in epididymis and is found on mouse, rat, monkey and human sperm suggests that CD52 has unknown but important roles in fertilization.

In human, all sperm are reported to possess CD52 on their surface, while in mouse, approximately a quarter of the population was found to react to anti-CD52 antibody (Fig. 3). The localization of CD52 on mouse sperm turned out to be different from human (midpiece in mouse versus whole sperm in human) and the site of CD52 transition from epididymal tissue to sperm seemed to be different between mouse and human (vas deferens in mouse versus in epididymis in human). It is not clear how CD52 is transferred from epididymal epithelium to sperm membrane. As a similar mechanism of transfer of membrane proteins to sperm, prostasomes are known in prostate and are speculated to transport membrane proteins to the sperm membrane (Ronquist & Brody 1985). Recently, exosome (Leblanc *et al.* 2006) in the epididymis, termed epididymosome, was reported to serve in epididymal maturation of sperm (Rejraji *et al.* 2006). CD52 might be transported through this secretion system and epididymosomes might be the origin of the speckled stainings observed in immunofluorescent analysis. Further investigation is awaited to learn if CD52 is transferred from epididymal epithelium to sperm plasma membrane or CD52-containing exosomes are only attaching on sperm membrane.

Although CD52 was found to be dispensable in fertilization, it does not mean that CD52 has no function in the system in wild-type mice. In the present paper, we could not find any apparent phenotype derived from the disruption of CD52 in immune system or in fertilization in mice kept under normal conditions. However, with combination to other gene disrupted mice, a severe phenotype might be expressed as in the case shown in Hox gene disruptions (Davis *et al.* 1995). In other words, various factors are known to be compensated by other factors, but their role becomes evident if the disruption is overlaid on another genetic background in which some other gene was disrupted (Nef *et al.* 2003). The CD52-disrupted mouse line may have such a characteristic. In order to make it possible to pursue further analysis of the role of CD52 *in vivo*, the CD52 disrupted mouse line was submitted to Riken BioResource center and is available to the scientific community.

Experimental procedures

Northern blot analysis

Northern hybridization was performed using 10 μg of total RNA extracted from various tissues of adult ICR mice. RNAs were separated by electrophoresis on agarose gels, transferred to Hybond-N$^+$ membranes (GE Healthcare Bio-Sciences Corp, Piscataway, NJ), and hybridized to ^{32}P-labeled probes at 60 °C overnight. Mouse *Cd52* and glyceraldehydes-3-phosphatate dehydrogenase (*Gapdh*) cDNAs were used as probes. The *Cd52* probe consisted of a cDNA fragment amplified from mouse epididymal total RNA by RT-PCR using 5′-TGAATTCTTCAAAGTGGCCTGCA GACTGTC-3′ and 5′-TGAATTCGCCATTGGCTGTCAAC TTTAGCC-3′ as primers.

Antibodies

Rabbit anti-mouse CD52 polyclonal antiserum was produced by immunization with mouse CD52 polypeptide (AASGTNKNST-STKKTPLKSG). Rat monoclonal antibody against mouse CD52 was a kind gift from Dr Nagahiro Minato (Kyoto University, Kyoto, Japan) (Kubota *et al.* 1990). A new monoclonal antibody against mouse IZUMO1 (Inoue *et al.* 2005) was produced by screening after immunization of whole mouse sperm to rat and termed Mab #125. Monoclonal antibodies against mouse ADAM2 (fertilin β 9D2.2) were purchased from Chemicon International, Inc. (Temecula, CA).

Immunohistochemistry

Epididymis and vas deferens were collected from adult *Cd52*$^{+/-}$ and *Cd52*$^{-/-}$ mice and embedded in a TissueTek O.C.T. compound (Sakura Finetechnical Co., Tokyo, Japan). Frozen sections (16 μm) prepared from these tissues were mounted on APS (aminosilane)

© 2008 The Authors
Journal compilation © 2008 by the Molecular Biology Society of Japan/Blackwell Publishing Ltd.

coated glass slides. Sperm from cauda epididymis or vas deferens were swum up in TYH medium and resuspended in PBS (Toyoda *et al.* 1971). Ejaculated sperm were collected from the uterus just after mating and resuspended in PBS. Sperm suspensions were mounted on glass slides and dried up. All samples were fixed in 4% paraformaldehyde/PBS for 30 min. After washing with PBS, slides were blocked with 10% New Born Calf Serum (NBCS)/PBS for 1 h and incubated with rat anti-mouse CD52 monoclonal antibody in 10% NBCS/PBS at 4 °C overnight. After washing with 10% NBCS/PBS containing 0.05% Tween-20, the slides were incubated with anti-rat IgG labeled with Alexa Fluor 488 (Invitrogen) in 10% NBCS/PBS for 1 h. After washing with PBS containing 0.05% Tween-20, the slides were observed under an Olympus IX-70 fluorescence microscope.

Immunoblot analysis

Immunoblot analysis was performed as described previously (Yamaguchi *et al.* 2006). Briefly, sperm from the epididymis and vas deferens were collected and incubated in lysis buffer containing 1% TritonX-100 for 20 min on ice. The testis, epididymis, and vas deferens were excised, minced, and homogenized in lysis buffer, and then placed on ice for 1 h. The sperm and tissue extracts were centrifuged, and the supernatants were collected. Proteins were separated by SDS-PAGE under reducing conditions and transferred electrophoretically to PVDF membranes. After blocking, blots were incubated with primary antibody overnight at 4 °C, and then incubated with horseradish-peroxidase conjugated goat anti-rabbit IgG, goat anti-mouse IgG and goat anti-rat IgG (GE Healthcare Bio-Sciences Corp.). The detection was performed using an ECL Western blotting detection kit (GE Healthcare).

Construction of the Cd52 gene disruption vector

A targeting vector was constructed using pPNT containing the Neo-resistance gene (*Neo*^{r}) as a positive selection marker and a herpes simplex virus thymidine kinase (*tk*) as a negative selection marker (Tybulewicz *et al.* 1991). A 2.1-kb *Not*I-*Sal*I fragment as a short arm and a 6.0-kb *Spe*I-*Kpn*I fragment as a long arm were obtained by PCR using genomic DNA in D3 embryonic stem (ES) cells as a template. The PCR primers used were as follows: 5′-GCGGCCGCAGTTAAAAGCACTTGTTGCAAGCCGGGCAG-3′ and 5′-TTTGTCGACGTGCGGCAGTATTAGGAGTGAACCCAGTAC-3′ for the short arm, 5′-GGACTAGTGGCCACTTTGAACCTGGCTGCTTTTTCTGC-3′ and 5′-TGGTACCAGAGGTCTCAACCTGTGGCTTGTGACCCAG-3′ for the long arm.

These two fragments were inserted into a pPNT vector and the targeting construct was linearized with *Not*I digestion. ES cells were electroporated and colonies were screened.

Generation of Cd52 mutant mice

G418-resistant colonies were amplified, and genomic DNA was prepared from them and screened by PCR analysis. Several of the recombinant ES cell lines carrying the disrupted *Cd52* allele were identified and subsequently used to generate chimeras by injection into blastocysts from C57BL/6 Cr mice (> 2 months old; Japan SLC, Inc., Shizuoka, Japan). Injected blastocysts were transferred to ICR pseudopregnant foster mothers, resulting in the birth of male chimeric mice. These mice were crossed with C57BL/6 to obtain F1 heterozygous offspring. *Cd52*-deficient mice were generated by the intercrossing F1 offspring. Mice used in this study were of B6; 129 mixed background.

All experiments were performed with the consent of the Animal Care and Use Committee of Osaka University.

Analysis of acrosome reaction and sperm motility

To investigate the influence of *Cd52* disruption on the sperm acrosome reaction, females from a transgenic mouse line which have enhanced green fluorescent protein in sperm acrosome (*Acr-EGFP*) were crossed with *Cd52*$^{-/-}$ males (Nakanishi *et al.* 1999). Double transgenic F1 offspring were intercrossed to generate *Cd52*$^{-/-}$ and *Acr-EGFP*$^{+/-}$. Sperm from double-transgenic mice were assayed as described in our previous paper (Inoue *et al.* 2003). Briefly, sperm were squeezed out from the incisions made in cauda epididymis or vas deferens and were suspended and incubated in TYH medium to induce a spontaneous acrosome reaction. Acrosomal statuses were analyzed from the acrosomal fluorescence by flow cytometer at 0, 30, 60, 120 and 180 min after insemination. Sperm motility was measured using epididymal sperm and automated Sperm Motility Analysis System (SMAS, Kaga Electronics Co. Ltd, Tokyo, Japan).

Sperm migration analysis

B6D2F1 females were superovulated by intraperitoneal injection of 5 units of equine chorionic gonadotropin followed 48 h later by 5 units of human chorionic gonadotropin (HCG). Superovulated females were caged together with test males 12 h after HCG injection, and the formation of vaginal plug was observed every 30 min. About 2 h after copulation, oviducts were excised together with the connective part of the uterus. To detect sperm in the uterotubal junction, the oviducts with attached uterus were fixed in 4% paraformaldehyde–PBS for 6 h, followed by washing with PBS, and were then prepared for frozen sections. Total of three females were examined using three males of each genotype.

Assessment of the fertilizing ability of Cd52-deficient mice

Female B6D2F1 mice (older than 8 weeks; Clea Japan Inc., Tokyo, Japan) were superovulated following intraperitoneal injections of eCG (Teikoku Zoki, Co. Ltd, Kanagawa, Japan) and hCG (Teikoku Zoki) at 48 h intervals. *Cd52*$^{+/-}$ or *Cd52*$^{-/-}$ males were mated with superovulated females 7 h after hCG injection. Eggs were recovered from females at their pronuclear stage and placed in a KSOM medium (Ho *et al.* 1995). Fertilization rates were assessed by pronuclear formation and subsequent 2-cell formation, observed by Olympus IX-70 microscope. *In vivo* fertilization was performed as previously described (Ikawa *et al.* 1997).

© 2008 The Authors
Journal compilation © 2008 by the Molecular Biology Society of Japan/Blackwell Publishing Ltd.

Acknowledgements

Authors thank Dr Nagahiro Minato (Kyoto University) for providing the antibody against CD52. Authors also thank Y. Maruyama, A. Kawai and Y. Koreeda for technical assistance with gene disruption. This work was supported in part by grants from the Ministry of Education, Science, Sports, Culture, and Technology, and the 21st Century 200 COE program from the Ministry of Education, Culture, Sports, Science and Technology of Japan.

References

Busso, D., Goldweic, N.M., Hayashi, M., Kasahara, M. & Cuasnicu, P.S. (2007) Evidence for the involvement of testicular protein CRISP2 in mouse sperm–egg fusion. *Biol. Reprod.* **76**, 701–708.

Calne, R., Moffatt, S.D., Friend, P.J., Jamieson, N.V., Bradley, J.A., Hale, G., Firth, J., Bradley, J., Smith, K.G. & Waldmann, H. (1999) Campath IH allows low-dose cyclosporine monotherapy in 31 cadaveric renal allograft recipients. *Transplantation* **68**, 1613–1616.

Cooper, T.G. (1995) Role of the epididymis in mediating changes in the male gamete during maturation. *Adv. Exp. Med. Biol.* **377**, 87–101.

Cornwall, G.A., Vreeburg, J.T., Holland, M.K. & Orgebin-Crist, M.C. (1990) Interactions of labeled epididymal secretory proteins with spermatozoa after injection of 35S-methionine in the mouse. *Biol. Reprod.* **43**, 121–129.

Davis, A.P., Witte, D.P., Hsieh-Li, H.M., Potter, S.S. & Capecchi, M.R. (1995) Absence of radius and ulna in mice lacking hoxa-11 and hoxd-11. *Nature* **375**, 791–795.

Hale, G. (2001) Cd52 (Campath1). *J. Biol. Regul. Homeost. Agents* **15**, 386–391.

Hale, G., Jacobs, P., Wood, L., *et al.* (2000) CD52 antibodies for prevention of graft-versus-host disease and graft rejection following transplantation of allogeneic peripheral blood stem cells. *Bone Marrow Transplant.* **26**, 69–76.

Ho, Y., Wigglesworth, K., Eppig, J.J. & Schultz, R.M. (1995) Preimplantation development of mouse embryos in KSOM: augmentation by amino acids and analysis of gene expression. *Mol. Reprod. Dev.* **41**, 232–238.

Ikawa, M., Wada, I., Kominami, K., Watanabe, D., Toshimori, K., Nishimune, Y. & Okabe, M. (1997) The putative chaperone calmegin is required for sperm fertility. *Nature* **387**, 607–611.

Inoue, N., Ikawa, M., Isotani, A. & Okabe, M. (2005) The immunoglobulin superfamily protein Izumo is required for sperm to fuse with eggs. *Nature* **434**, 234–238.

Inoue, N., Ikawa, M., Nakanishi, T., Matsumoto, M., Nomura, M., Seya, T. & Okabe, M. (2003) Disruption of mouse CD46 causes an accelerated spontaneous acrosome reaction in sperm. *Mol. Cell. Biol.* **23**, 2614–2622.

Kim, T., Oh, J., Woo, J.M., Choi, E., Im, S.H., Yoo, Y.J., Kim, D.H., Nishimura, H. & Cho, C. (2006) Expression and relationship of male reproductive ADAMs in mouse. *Biol. Reprod.* **74**, 744–750.

Kirchhoff, C. (1996) CD52 is the "major maturation-associated" sperm membrane antigen. *Mol. Hum. Reprod.* **2**, 9–17.

Kirchhoff, C. & Schroter, S. (2001) New insights into the origin, structure and role of CD52: a major component of the mammalian sperm glycocalyx. *Cells Tissues Organs* **168**, 93–104.

Kubota, H., Okazaki, H., Onuma, M., Kano, S., Hattori, M. & Minato, N. (1990) Identification and gene cloning of a new phosphatidylinositol-linked antigen expressed on mature lymphocytes. Down-regulation by lymphocyte activation. *J. Immunol.* **145**, 3924–3931.

Leblanc, P., Alais, S., Porto-Carreiro, I., Lehmann, S., Grassi, J., Raposo, G. & Darlix, J.L. (2006) Retrovirus infection strongly enhances scrapie infectivity release in cell culture. *EMBO J.* **25**, 2674–2685.

Nakanishi, T., Ikawa, M., Yamada, S., Parvinen, M., Baba, T., Nishimune, Y. & Okabe, M. (1999) Real-time observation of acrosomal dispersal from mouse sperm using GFP as a marker protein. *FEBS Lett.* **449**, 277–283.

Nef, S., Verma-Kurvari, S., Merenmies, J., Vassalli, J.D., Efstratiadis, A., Accili, D. & Parada, L.F. (2003) Testis determination requires insulin receptor family function in mice. *Nature* **426**, 291–295.

Okabe, M. & Cummins, J.M. (2007) Mechanisms of sperm-egg interactions emerging from gene-manipulated animals. *Cell. Mol. Life Sci.* **64**, 1945–1958.

Qin, X., Dobarro, M., Bedford, S.J., Ferris, S., Miranda, P.V., Song, W., Bronson, R.T., Visconti, P.E. & Halperin, J.A. (2005) Further characterization of reproductive abnormalities in mCd59b knockout mice: a potential new function of mCd59 in male reproduction. *J. Immunol.* **175**, 6294–6302.

Qin, X., Krumrei, N., Grubissich, L., Dobarro, M., Aktas, H., Perez, G. & Halperin, J.A. (2003) Deficiency of the mouse complement regulatory protein mCd59b results in spontaneous hemolytic anemia with platelet activation and progressive male infertility. *Immunity* **18**, 217–227.

Rejraji, H., Sion, B., Prensier, G., Carreras, M., Motta, C., Frenoux, J.M., Vericel, E., Grizard, G., Vernet, P. & Drevet, J.R. (2006) Lipid remodeling of murine epididymosomes and spermatozoa during epididymal maturation. *Biol. Reprod.* **74**, 1104–1113.

Ronquist, G. & Brody, I. (1985) The prostasome: its secretion and function in man. *Biochim. Biophys. Acta* **822**, 203–218.

Sullivan, R., Saez, F., Girouard, J. & Frenette, G. (2005) Role of exosomes in sperm maturation during the transit along the male reproductive tract. *Blood Cells Mol. Dis.* **35**, 1–10.

Tone, M., Nolan, K.F., Walsh, L.A., Tone, Y., Thompson, S.A. & Waldmann, H. (1999) Structure and chromosomal location of mouse and human CD52 genes. *Biochim. Biophys. Acta* **1446**, 334–340.

Topfer-Petersen, E. (1999) Carbohydrate-based interactions on the route of a spermatozoon to fertilization. *Hum. Reprod. Update* **5**, 314–329.

Toshimori, K. (2003) Biology of spermatozoa maturation: an overview with an introduction to this issue. *Microsc. Res. Tech.* **61**, 1–6.

Toyoda, Y., Yokoyama, M. & Hoshi, T. (1971) Studies on the fertilization of mouse egg *in vitro*. *Jpn. J. Anim. Reprod.* **16**, 147–151.

Tulsiani, D.R. (2006) Glycan-modifying enzymes in luminal fluid of the mammalian epididymis: an overview of their potential role in sperm maturation. *Mol. Cell. Endocrinol.* **250**, 58–65.

© 2008 The Authors
Journal compilation © 2008 by the Molecular Biology Society of Japan/Blackwell Publishing Ltd.

Tybulewicz, V.L., Crawford, C.E., Jackson, P.K., Bronson, R.T. & Mulligan, R.C. (1991) Neonatal lethality and lymphopenia in mice with a homozygous disruption of the c-abl proto-oncogene. *Cell* **65**, 1153–1163.

Vreeburg, J.T., Holland, M.K., Cornwall, G.A. & Orgebin-Crist, M.C. (1990) Secretion and transport of mouse epididymal proteins after injection of 35S-methionine. *Biol. Reprod.* **43**, 113–120.

Williams, R.M., Graham, J.K. & Hammerstedt, R.H. (1991) Determination of the capacity of ram epididymal and ejaculated sperm to undergo the acrosome reaction and penetrate ova. *Biol. Reprod.* **44**, 1080–1091.

Yamaguchi, R., Yamagata, K., Ikawa, M., Moss, S.B. & Okabe, M. (2006) Aberrant distribution of ADAM3 in sperm from both Angiotensin-converting enzyme (Ace)- and Calmegin (Clgn)-deficient mice. *Biol. Reprod.* **75**, 760–766.

Yeung, C.H., Perez-Sanchez, F., Schroter, S., Kirchhoff, C. & Cooper, T.G. (2001) Changes of the major sperm maturation-associated epididymal protein HE5 (CD52) on human ejaculated spermatozoa during incubation. *Mol. Hum. Reprod.* **7**, 617–624.

Received: 2 February 2008
Accepted: 13 May 2008

Supplementary material

The following supplementary materials are available for this article online:

Figure S1 Cell populations of thymocytes and splenocytes in terms of expression of CD antigens.

This material is available as part of the online article from:
http://www.blackwell-synergy.com/doi/abs/10.1111/j.1365-2443.2008.01210.x
(This link will take you to the article abstract).

Please note: Blackwell Publishing are not responsible for the content or functionality of any supplementary materials supplied by the authors. Any queries (other than missing material) should be directed to the corresponding author for the article.

© 2008 The Authors
Journal compilation © 2008 by the Molecular Biology Society of Japan/Blackwell Publishing Ltd.

Am J Physiol Endocrinol Metab 295: E1349–E1357, 2008.
First published October 7, 2008; doi:10.1152/ajpendo.90704.2008.

Bis deficiency results in early lethality with metabolic deterioration and involution of spleen and thymus

Dong-Ye Youn,[1]* Dong-Hyoung Lee,[1]* Mi-Hyun Lim,[1] Jung-Sook Yoon,[2] Ji Hee Lim,[2] Seung Eun Jung,[1] Chung Eun Yeum,[3] Cheol Whee Park,[2] Ho-Joong Youn,[2] Jae-Seon Lee,[4] Seong-Beom Lee,[3] Masahito Ikawa,[5] Masaru Okabe,[5] Yoshihide Tsujimoto,[6,7] and Jeong-Hwa Lee[1]

[1]Department of Biochemistry, [2]Department of Internal Medicine, and [3]Department of Pathology, College of Medicine, Catholic University of Korea and [4]Division of Radiation Cancer Research, Korea Institute of Radiological and Medical Science, Seoul, Korea; and [5]Genome Information Research Center, Research Institute for Microbial Diseases, Osaka University, [6]Department of Medical Genetics, Laboratory of Molecular Genetics, Osaka University Medical School, and [7]Solution-Oriented Research for Science and Technology, Japan Science and Technology Agency, Osaka, Japan

Submitted 18 August 2008; accepted in final form 25 September 2008

Youn DY, Lee DH, Lim MH, Yoon JS, Lim JH, Jung SE, Yeum CE, Park CW, Youn HJ, Lee JS, Lee SB, Ikawa M, Okabe M, Tsujimoto Y, Lee JH. Bis deficiency results in early lethality with metabolic deterioration and involution of spleen and thymus. *Am J Physiol Endocrinol Metab* 295: E1349–E1357, 2008. First published October 7, 2008; doi:10.1152/ajpendo.90704.2008.— Bcl-2 interacting cell death suppressor (Bis), also known as Bag3 or CAIR-1, is involved in antistress and antiapoptotic pathways. In addition to Bcl-2, Bis binds to several proteins, suggesting it has diverse functions in normal and pathological conditions. To better define the physiological function of Bis in vivo, we developed *bis*-deficient mice with a *cre-loxP* system. Targeted disruption of exon 4 of the *bis* gene was demonstrated by Southern blotting and PCR, and Western blotting showed that no intact or truncated Bis protein was synthesized in $bis^{-/-}$ mice. While heterozygotes were fertile and appeared normal, Bis-deficient mice showed growth retardation and died by 3 wk after birth. The relative weight of the thymus and spleen was reduced and the total numbers of white blood cells, splenocytes, and thymocytes were significantly reduced compared with wild-type littermates. Serum profiles indicated significant hypoglycemia as well as decrease in triglyceride and cholesterol levels. Expression profiles of metabolic genes indicated that gluconeogenesis and β-oxidation are activated in the liver of $bis^{-/-}$ mice. This activation, as well as a decrease in peripheral fat and an induction of fatty liver, appears to be an adaptive response to hypoglycemia. Our study reveals that the absence of Bis has considerable influences on postnatal growth and survival, possibly due to a nutritional impairment.

bis; knockout; hypoglycemia

THE BCL-2 INTERACTING DEATH SUPPRESSOR (*bis*) gene has been identified as encoding a Bcl-2 binding protein in protein interaction techniques (18). Bis has also been reported as Bag3 and CAIR-1, which bind to heat shock protein (HSP)70 and PLC-γ, respectively (7, 33). The ability of Bis to bind to several proteins suggests that it has distinct functions depending on its cellular environment. A possible role for Bis in modulating cell death was revealed in in vitro DNA transfection experiments in which Bis was shown to significantly enhance the antiapoptotic function of Bcl-2 (18). Supporting this, Bis has also been shown to be specifically expressed or overexpressed in several cancers, including pancreatic cancer, thyroid carcinoma, and some leukemia (1, 5, 21, 27, 28). Furthermore, the downmodulation of Bis results in an increased susceptibility for the induction of apoptosis in cancer cells (1, 5, 26). Bis has been also proposed as an antistress protein, based on the upregulation of its expression, concomitant with HSP70, in cells exposed to stressful stimuli such as heat shock or heavy metals (21, 23). In addition to the stressful conditions given for cellular levels, the expression of Bis is significantly upregulated in several in vivo disease models such as stroke and seizure models (19, 20, 31). Moreover, Bis is robustly expressed in reactive astrocytes in areas of gliosis in the brain of human immunodeficiency virus (HIV) encephalopathy patients (29). Light damage also increases the expression of Bis in the mouse retina (4). These results suggest that the expression of Bis may be induced to protect cells from stressful conditions, but the persistent and/or uncontrolled expression of Bis may contribute to the progression of cancer.

In addition to its possible role as a stress- or survival-related protein, Bis has been implicated to have other cellular functions. Overexpression of Bis promotes the differentiation of human promyelocytic cells and cell cycle arrest (32). Roles for Bis in cell adhesion and migration have been recently reported by separate groups, although their results differ: in one study overexpression of Bis is shown to inhibit the migration and adhesion of breast cancer cell lines, whereas in the other study *bis*-deficient fibroblasts have reduced motility and delayed formation of focal adhesion complex (12, 14). These results suggest that complex mechanisms are involved in the regulation of cellular motility by Bis. Furthermore, cytoplasmic Bis protein modulates the transcription of the HIV-1 gene and the replication of the varicella-zoster virus (15, 29). Therefore, it appears that Bis exerts diverse functions in pathophysiological conditions in vivo, which may be partly ascribed to its ability to interact with several known and yet to be identified proteins.

To better define the function of Bis in vivo, we developed *bis*-deficient mice with a *cre-loxP* system targeting exon 4. Here we show that disruption of exon 4 of the *bis* gene by homologous recombination led to a complete inhibition of Bis protein synthesis, which resulted in serious hypoglycemia, a fatty liver, and 100% lethality before 3 wk of age. Bis-deficient mice also exhibited a significant involution of the spleen and thymus. Our results are inconsistent with a previous study in

* D.-Y. Youn and D.-H. Lee contributed equally to this work.
Address for reprint requests and other correspondence: J.-H. Lee, 505 Banpo-Dong, Seocho-gu, Seoul 137-701, Korea (e-mail: leejh@catholic.ac.kr).

The costs of publication of this article were defrayed in part by the payment of page charges. The article must therefore be hereby marked "*advertisement*" in accordance with 18 U.S.C. Section 1734 solely to indicate this fact.

0193-1849/08 $8.00 Copyright © 2008 the American Physiological Society

Downloaded from ajpendo.physiology.org on January 18, 2009

which retrovirus-targeted deletion of the *bis* gene resulted in massive degeneration of myofibrils with apoptotic features in heart and skeletal muscles and no abnormalities in other organs (10). Possible explanations for the differences observed in *bis*-deficient mice in the previously published study and the present study are discussed below.

METHODS

Construction of targeting vector and generation of bis-mutant mice. A 6,018-bp genomic clone that includes coding exons 3 and 4 of the *bis* gene (nucleotides 17173-23356 from the start codon) was cloned from D3 mouse embryonic stem (ES) cells as the long arm and introduced into a pMulti-ND 1.0 vector with *Pme*I and *Pac*I sites (11). The *loxP* sequences were inserted into an *Eco*RV site located between exon 3 and exon 4. For homologous recombination, the downstream short arm spanning nucleotides 23357-27370 was also cloned and introduced into a *Not*I site of a pMulti vector. The resulting *Pme*I-digested targeting vector was electroporated into D3 ES cells derived from 129Sv and screened for neomycin resistance. Of 98 neomycin-resistant clones, four clones were shown to have the desired homologous recombination as determined by Southern blotting with two different probes for the 5′ and 3′ regions external to the targeting vector and one probe for the neomycin sequences. Four homologous recombinant ES clones were independently injected into C57B6 blastocysts to generate chimeric mice. Male chimera derived from one ES clone transmitted the recombinant allele to the next generation. To generate heterozygous mutants with deletion of exon 4 of the *bis* gene on one chromosome, the germ line-transmitted male mice were mated with *CAG-cre* C57B6 females.

All research procedures involving animals were performed in accordance with the Laboratory Animals Welfare Act, the *Guide for the Care and Use of Laboratory Animals*, and the Guidelines and Policies for Rodent Experiments provided by the Institutional Animal Care and Use Committee (IACUC) at the College of Medicine, Catholic University of Korea and were reviewed and approved by the IACUC.

Southern blotting and allele-specific genomic PCR. Genomic DNA extracted from wild-type or *bis*-mutant mice livers was digested with *Bam*HI enzyme and electrophoresed through 0.8% agarose. After transfer onto nylon membrane by capillary blotting, the membrane was hybridized with a digoxigenin (DIG)-labeled specific DNA probe and then immunodetected with alkaline phosphatase-conjugated anti-DIG antibody and a chemiluminescent substrate (Roche Applied Science, Mannheim, Germany) as described previously (17). The following primers were used to incorporate DIG-11 dUTP for the DNA probes: 5′-TGA GGT AAG AAG AGA CCC AGA GAC (forward primer) and 5′-TAC AGA CGT AGG AAA CAC ATC TCC (reverse primer).

PCR reactions were also performed to detect the truncated *bis* allele in genomic DNA with two sets of primers, 5′-TGA GAG CCA GCA TGC TGT TTC ATT and 5′-TGG CCC TCA GGG GAC AAC CTG CAG designed to amplify a region of 500 bp in the wild-type allele and 5′-CTT TCA AGG ATT TAA CTT ATC TGA CCA and 5′-ACA GCA AGC ATA TTC CTC TAC CTA AG to amplify a 3,003-bp product in the wild-type allele and a 1,043-bp product in the post-*cre* allele. PCR products were electrophoresed on a 1.5% agarose gel and visualized with ethidium bromide staining.

Western blotting. Proteins from various tissues of wild-type or *bis*-mutant mice were prepared and Western blotting was performed as described previously (17). To analyze Bis expression, the blotted membranes were incubated with polyclonal antibodies against the COOH-terminal half of human Bis (306-575 aa) (18) or against whole human Bis (Abnova, Taiwan, Taipei). Polyclonal antibodies raised in rabbit against the NH_2-terminal of human Bis (48-63 aa) (Peptron, Daejeon, Korea) were also used to detect smaller truncated Bis proteins. Antibodies for HSP70 and Bcl-2 were purchased from BD Biosciences (San Jose, CA) and Santa Cruz Biotechnology (Santa Cruz, CA), respectively.

Complete blood count and assay of metabolites in blood and liver. The complete blood count was determined with a Hemavet 850 automated hematologic analyzer (CDC Technologies, Oxford, CT). The concentration of glucose in the blood was determined by Hemocue Glucose 201 + (Hemocue, Angelholm, Sweden). Plasma concentration of insulin was measured with a mouse insulin enzyme-linked immunoabsorbent assay kit (Linco Research, Erie, PA). Measurements of triglyceride, free fatty acid, and cholesterol in the serum and in the liver were performed with the Triglyceride E-test, NEFA-HR (2), and Labassay Cholesterol, respectively (Wako Pure Chemical Industries, Osaka, Japan).

Histological analysis. Paraffin sections (10 μm) from various organs were processed for hematoxylin and eosin (H & E) staining. Frozen liver sections (6 μm) were fixed with 10% formalin, stained with 0.5% Oil Red O, and counterstained with Mayer's hematoxylin. To examine the state of apoptosis in situ in muscles, a terminal deoxynucleotidyl transferase-mediated dUTP nick end labeling (TUNEL) assay was also performed with the ApopTag Peroxidase In Situ Apoptosis Detection Kit S7100 (Chemicon, Temecula, CA). Specimens were examined under a light microscope (Axioskop40, Carl Zeiss, Gottingen, Germany). For electron microscopy, the tissue samples were fixed with 2.5% glutaraldehyde for 1 h. After fixation, the samples were postfixed in 1% O_5O_4, dehydrated in ethanol, and embedded in Epon 812 (Polysciences, Warrington, PA). Ultrathin sections were contrasted with uranyl acetate and lead citrate. Sections were examined in a JEM 1010 CX transmission electron microscope (JEOL, Akishima, Japan).

RNA extraction and quantitative real-time PCR. Total RNA from liver was isolated with RNA-Bee (Tel-Test, Friendswood, TX). cDNA was synthesized from 2 μg of total RNA with AccuPower Cycle Script (dN6) (Bioneer, Daejeon, Korea). mRNA levels of genes involved in glucose and lipid metabolism were measured by quantitative real-time PCR using a cDNA template and appropriate primers as previously described (Refs. 9, 25, 34; Supplemental Table S1).[1] Quantitative real-time PCR was performed with the IQ5 Real Time PCR detection System (Bio-Rad Laboratories, Hercules, CA) and iQ TM SYBR Green Supermix (Bio-Rad Laboratories). Relative levels of PCR products were determined after normalizing to an endogenous cyclophilin control.

Statistical analysis. The number of mice in each experimental group is indicated in Figs. 2 and 3. A two-tailed Student's *t*-test was used to calculate *P* values. All values are presented as means ± SE. Differences were considered significant if $P < 0.05$.

RESULTS

Targeting the bis gene and generation of bis-mutant mice. The coding region of mouse *bis* consists of four exons. The 315-amino acid peptide encoded by exon 4 includes the bag domain and a proline-rich region, which are required for the regulation of HSP70 chaperone activity and cellular motility, respectively (14, 33). To disrupt exon 4, we generated a targeting vector in which exon 4 was bracketed by *loxP* sites as shown in Fig. 1A. The germ line-transmitted male mice were obtained and mated with *CAG-cre* C57B6 females as described in METHODS. The resulting heterozygous male *bis* mutants were backcrossed into C57B6 females for more than eight generations to minimize the contribution of the 129Sv genetic background of ES cells on the phenotype of *bis* mutants. Male and female *bis* heterozygotes were interbred to generate homozygous mice. In $bis^{-/-}$ mice, the *loxP* sites and the intervening

[1] The online version of this article contains supplemental material.

Downloaded from ajpendo.physiology.org on January 18, 2009

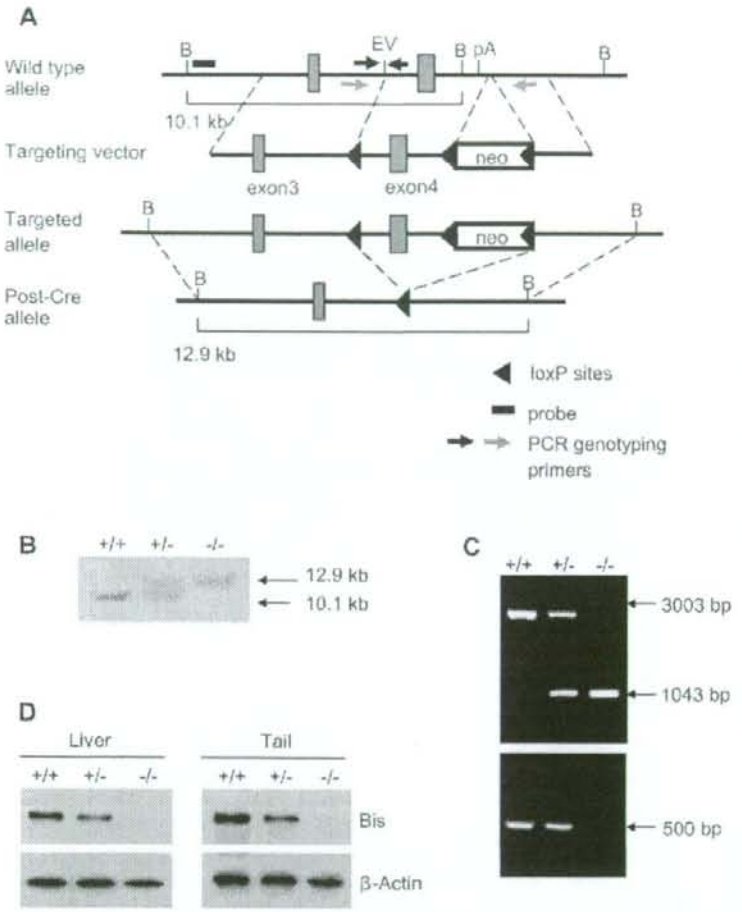

Fig. 1. Targeted disruption of the *bis* gene. *A*: schematic representation of a part of the *bis* genomic locus, targeting vector, and mutant allele. The targeting vector includes the 5′ long arm, the neomycin-resistant gene (*neo*), and the 3′ short arm for homologous recombination. Exon 4, as well as *neo*, was flanked by *loxP* sequences, shown as arrowheads. The sizes of *Bam*HI DNA fragments are indicated beneath the wild-type allele and post-*cre* allele. The 5′ external probe used for Southern blotting is shown as a black square. The small black and gray arrows indicate the locations of the primers used for genotyping. B, *Bam*HI; EV, *Eco*RV; pA, poly A. *B*: Southern blot analysis. Genomic DNA (10 μg) was extracted from liver of mice of the indicated *bis* genotypes. Hybridization of genomic DNA with the external probe, shown in *A*, revealed a 10.1-kb *Bam*HI fragment for wild-type allele and a 12.9-kb *Bam*HI fragment for knockout allele, corresponding to the deletion of a *Bam*HI site and exon 4 by *Cre* excision. *C*: PCR analysis. Genomic DNA was isolated from mouse tails, and PCR screening was performed with 2 pairs of primers, indicated in *A*. A pair of primers (gray arrows in *A*) were designed to produce a 3,003-bp product from the wild-type allele and a 1,043-bp product from the post-*cre* allele. Another pair of primers (black arrows in *A*) failed to amplify a 500-bp product in homozygous $bis^{-/-}$ mice because of the deletion of a section of DNA that contained the reverse primer site. *D*: Western blotting using whole protein extracts from liver and tail revealed that there is no intact Bis protein in $bis^{-/-}$ mice.

DNA, including a *Bam*HI site, were deleted, generating a 12.9-kb fragment of *Bam*HI compared with a 10.1-kb fragment in $bis^{+/+}$ mice, as shown in a Southern blot using genomic DNA extracted from the tail (Fig. 1*B*). PCR analysis using two pairs of primers, upstream and downstream of either the first *loxP* site or all three *loxP* sites, also confirmed the elimination of the DNA fragment flanked by the *loxP* sites (Fig. 1*C*). Expression of the 80-kDa Bis protein was reduced in $bis^{+/-}$ heterozygous and undetectable in $bis^{-/-}$ homozygous mouse liver tissues in a Western blot with Bis-specific antibody against the COOH terminus of Bis (Fig. 1*D*). Neither anti-Bis antibodies raised against whole peptides of Bis nor anti-Bis antibodies specific for its NH_2 terminus showed any smaller size of Bis protein products in heterozygous and homozygous tissues, excluding the possibility of the presence of truncated Bis protein composed of exon 1 from exon 3 (Supplemental Fig. S1). Therefore, disruption of exon 4 of the *bis* gene resulted in the complete inhibition of synthesis of both intact Bis protein and aberrant forms of Bis.

General characteristics of $bis^{-/-}$ mice. The $bis^{-/-}$ offspring were born roughly in a Mendelian ratio: 67 $bis^{-/-}$ homozygous, 135 $bis^{+/-}$ heterozygous, and 75 $bis^{+/+}$ wild type. While $bis^{+/-}$ heterozygous mice appeared normal and were fertile, all $bis^{-/-}$ homozygous mice died before 3 wk of age. As shown in Fig. 2*A*, the difference in body weight between homozygous $bis^{-/-}$ and both heterozygous and wild-type mice was imperceptible at birth but became noticeable within 1 wk after birth and obvious until 12–13 days after birth. Thereafter, the $bis^{-/-}$ mice failed to gain weight and began to gradually lose body weight before they died. Apparently, the thymus and spleen of $bis^{-/-}$ mice shrank dramatically to 51% and 36% of wild type, respectively, in terms of weight per total body weight at 16 days after birth (Fig. 2, *C* and *D*). The involution of spleen in *bis*-deficient mice appeared before that of thymus, showing a reduction of relative weight to 50% of wild type at 14 days after birth but no reduction of thymus (Fig. 2*E*). In addition, the external surface of livers from $bis^{-/-}$ mice, which were 80% of the relative weight of wild-type livers, appeared pale (Fig. 2, *C*

Downloaded from ajpendo.physiology.org on January 18, 2009

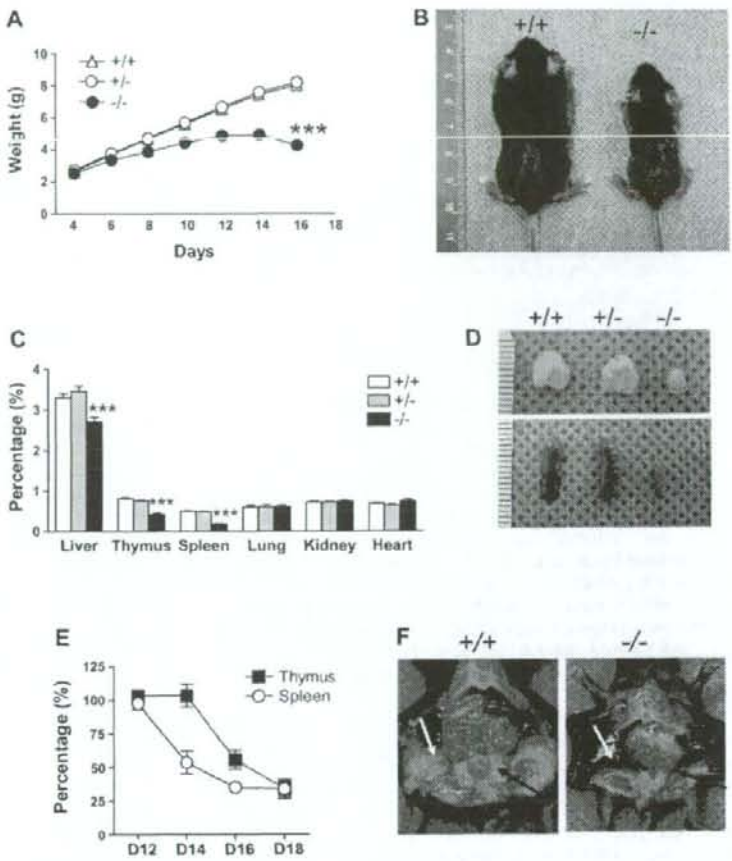

Fig. 2. Characterization of *bis*-deficient mice. *A*: growth of wild-type and $bis^{-/-}$ mice. Offspring generated from heterozygous intercrosses of $bis^{+/-}$ mice were weighed at 2-day intervals from 4 days until 16 days after birth. [n = 46 for wild-type (+/+), 104 for $bis^{+/-}$, 36 for $bis^{-/-}$]. ***$P < 0.001$, compared with wild-type littermates. *B*: representative picture showing significant growth retardation of a $bis^{-/-}$ mouse compared with a wild-type littermate at 16 days of age. *C*: relative weight of each organ to total body weight as shown as %. The ratios of thymus and spleen weight to total body weight in homozygous $bis^{-/-}$ mice were significantly decreased compared with those in wild-type and heterozygous mice older than 16 days of age (n = 15 for $^{+/+}$, 12 for $bis^{+/-}$, 16 for $bis^{-/-}$). ***$P < 0.001$, compared with wild-type littermates. *D*: representative morphology of thymus (*top*) and spleen (*bottom*) at 16 days of age showing notable reduction in size in *bis*-deficient mice. *E*: the decreased size of the thymus and spleen in *bis*-deficient mice was not obvious until age 12 days; thereafter, shrinkage of the spleen occurred before that of the thymus. The relative weight of the thymus and the spleen in $bis^{-/-}$ mice was compared with that of wild-type littermates, and the ratio is shown as %. The data are means ± SE. The number of animals measured each day is 4, 6, 8, and 5 for days (D)12, 14, 16, and 18, respectively. *F*: reduction of subcutaneous fat (white arrow) and periepididymal fat (black arrow) in a male *bis*-deficient mouse at 16 days of age compared with a wild-type male littermate.

and *F*). Notably, the subcutaneous fat and the perigonadal fat were severely reduced in $bis^{-/-}$ mice compared with wild-type mice at day 16 (Fig. 2*F*).

Decreased number of thymocytes, splenocytes, and leukocytes in peripheral blood of bis-deficient mice. As predicted from the reduced size of the thymus and spleen of *bis*-deficient mice, the number of splenocytes and thymocytes was significantly decreased, about one-tenth and one-fifth compared with wild type in the spleen and thymus, respectively, at ≥16 days of age (Table 1). The *bis*-deficient mice also had a >50% decrease in the number of total peripheral leukocytes, but the proportion of neutrophils and lymphocytes was not significantly different from that in wild-type littermates (Table 1). The difference in the number of red blood cells and platelets in *bis*-deficient and wild-type mice was insignificant.

Bis deficiency caused hypoglycemia and hepatic steatosis. The reduction in perigonadal and subcutaneous fat in $bis^{-/-}$ mice suggested that the mice suffered from malnutrition and led us to inspect the metabolic parameters in the serum. As shown in Table 2, serum glucose levels were decreased to one-third the levels of wild type in $bis^{-/-}$ mice. Insulin levels were also lower in *bis*-deficient mice than in $bis^{+/+}$ mice, showing that the hypoglycemia observed in the $bis^{-/-}$ mice was not due to high levels of insulin. Total cholesterol and triglyceride levels were also significantly decreased in *bis*-deficient mice, 60% and 26% of those in wild-type littermates, respectively. The levels of β-hydroxybutyrate, a product of

Table 1. *Comparison of cellularity in spleen and thymus and total blood cell counts in wild-type and bis-deficient mice*

	$bis^{+/+}$	$bis^{-/-}$
Splenocytes, $\times 10^6$	46.2 ± 11.4 (7)	4.67 ± 1.12 (12)*
Thymocytes, $\times 10^7$	16.7 ± 2.79 (7)	2.97 ± 0.87 (12)†
RBC, $\times 10^{12}$/l	6.18 ± 0.18 (9)	6.77 ± 0.16 (13)*
Platelets, $\times 10^9$/l	333 ± 47.2 (9)	329 ± 48.2 (13)
WBC, $\times 10^9$/l	6.63 ± 0.63 (9)	2.76 ± 0.34 (13)‡
Neutrophils	1.72 ± 0.25 (9)	0.71 ± 0.13 (13)†
Lymphocytes	3.98 ± 0.32 (9)	1.63 ± 0.17 (13)‡
Others	0.84 ± 0.18 (9)	0.42 ± 0.07 (13)*

Values are means ± SE for numbers of animals in parentheses. RBC, red blood cells; WBC, white blood cells; Others, monocytes, eosinophils, and basophils. *$P < 0.05$, †$P < 0.01$, ‡$P < 0.001$ compared with $bis^{+/+}$ littermates.

Downloaded from ajpendo.physiology.org on January 18, 2009

Table 2. *Profile of serum metabolites of wild-type and bis-deficient mice*

Parameter	$bis^{+/+}$	$bis^{-/-}$
Glucose, mg/dl	212.9 ± 11.9 (13)	71.46 ± 4.03 (17)‡
Insulin, pg/ml	768.5 ± 119.7 (7)	282.9 ± 77.5 (11)†
TAG, mg/dl	158.6 ± 21.3 (7)	41.7 ± 11.7 (7)‡
FFA, meq/l	1.2 ± 0.2 (7)	1.0 ± 0.2 (7)
Cholesterol, mg/dl	137.7 ± 11.6 (7)	80.4 ± 5.3 (7)‡
β-Hydroxybutyrate, mmol/l	2.80 ± 0.56 (3)	6.44 ± 1.30 (3)*

Results were obtained from mice at age 16 days and expressed as means ± SE for numbers of animals indicated in parentheses. TAG, triglyceride; FFA, free fatty acids. *$P < 0.05$, †$P < 0.01$, ‡$P < 0.001$ compared with wild-type littermates.

ketogenesis, were increased in $bis^{-/-}$ mice to ~2.5-fold above wild-type levels.

Although no obvious changes were observed by H & E staining (data not shown), Oil Red O staining revealed marked accumulation of lipids throughout the $bis^{-/-}$ liver tissues (Fig. 3*A*). Ultrastructural analysis of the hepatocytes of $bis^{-/-}$ mice revealed the presence of enlarged lipid particles and an increased number of lipid particles (Fig. 3*B*). The lipid contents of the $bis^{-/-}$ livers were analyzed to identify the type of accumulated lipids. In contrast to the serum profile of free fatty acids (FFA), which showed no difference between $bis^{-/-}$ and $bis^{+/+}$ mice, hepatic FFA levels in $bis^{-/-}$ livers were increased to twofold compared with wild-type littermates. $bis^{-/-}$ mice also had 2.8-fold and 3.4-fold increases in hepatic triglyceride and cholesterol levels, respectively, compared with control mice (Fig. 3*C*).

Quantitative RT-PCR revealed increased hepatic expression of mRNAs involved in gluconeogenesis in $bis^{-/-}$ mice, including glucose 6-phosphatase (G6Pase) and phosphoenolpyruvate carboxykinase (PEPCK) (Fig. 3*D*). The expression of several lipogenic genes, including fatty acid synthase (FAS) and stearoyl-CoA desaturase-1 (SCD-1), was markedly diminished, suggesting that de novo synthesis of fatty acids is inhibited in $bis^{-/-}$ mice (Fig. 3*D*). In addition, several hepatic genes involved in β-oxidation, such as carnitine palmitoyltransferase I (CPT-1) and medium-chain acyl-CoA dehydrogenase (MCAD), were induced in $bis^{-/-}$ mice (Fig. 3*D*). Thus hepatic steatosis in $bis^{-/-}$ mice is likely due to fatty acid delivery that exceeds the capacity for hepatic fatty acid oxidation to generate energy for gluconeogenesis, which are the typical metabolic changes in response to fasting (3, 8).

Bis deficiency caused no prominent apoptosis in diaphragm and cardiomyocytes. Bis is highly expressed in skeletal muscles (18), and a previous study with mice in which the *bis* gene had been disrupted by retroviral insertion described that, as the only abnormal finding, *bis*-deficient mice developed a fulminant myopathy characterized by noninflammatory myofibrillar degeneration with apoptotic features (10). However, in our model, no significant differences in H & E staining were found between the skeletal muscles from wild-type and *bis*-deficient mice (Fig. 4*A*), and the ventricular cardiomyocytes revealed similar frequencies in cells positive for TUNEL staining in wild-type and $bis^{-/-}$ mice (Fig. 4*B*). The diaphragm of $bis^{-/-}$ mice revealed a slight increase in TUNEL-positive apoptotic cells (Fig. 4*C*) but not as prominent as previously described by Homma et al. (10). When wild-type mice with body weight similar to $bis^{-/-}$ mice at day 12 after birth were fasted for 48 h, TUNEL-positive cells were increased in the diaphragm compared with feeding control (data not shown). Thus the increase of apoptotic cells in the diaphragm of $bis^{-/-}$ mice might represent a nutritionally insufficient status rather than acceleration of apoptosis due to the absence of Bis. Although no considerable abnormalities were noted in H & E staining, ultrastructures of muscles from *bis*-deficient mice exhibited discontinuous arrangement of myofibrils with thick and short Z bands but nuclei preserved normal morphology (Fig. 4*D*). Previous reports showed the colocalization of Bis with Z-disk proteins such as α-actinin and desmin (10). Thus Bis protein may contribute to preservation of the architecture of myofibrils, especially the integrity of Z bands, rather than the viability of myocytes.

DISCUSSION

Bis is expressed in various tissues, including skeletal muscle, heart, and kidney, and known to bind with several proteins, suggesting that it has diverse physiological functions. Using a *cre-loxP* system, we generated *bis* knockout mice and showed that these mice died within 3 wk after birth with metabolic derangements such as hypoglycemia and hepatic steatosis and significant reduction in the cellularity of the thymus and spleen. A previous study with mice in which the *bis* gene had been disrupted by retroviral insertion also reported premature death before weaning, although these mice died ~1 wk later than the time of death we observed (10). Furthermore, the previous study described severe degeneration and apoptosis in skeletal muscles and myocardium and no evidence of abnormality in other organs (10). In the present study, we found that the skeletal muscle fibers from $bis^{-/-}$ mice were irregular and smaller than those of wild-type littermates but found no evidence for massive apoptosis in the diaphragm, quadriceps, and cardiac muscles (Fig. 4 and data not shown). In addition, several of the phenotypes we report here, such as shrinkage of lymphoid organs and perturbations in metabolic homeostasis, were not observed in the previous report.

At present, the precise reasons for the differences in the phenotypes of our model and the previous model are not entirely clear. The method used for gene targeting may contribute to the different phenotypes observed. The previous *bis*-deficient model was developed with ES clones that had been mutagenized by retroviral insertion (10); our *bis*-deficient mice model was developed by precise deletion of exon 4 of the *bis* gene with a *Cre-loxP* system. Although the previous report does not describe which part of the *bis* gene was disrupted by retroviral insertion, partial disruption of the *bis* gene may have resulted in the expression of truncated Bis protein products, and these may have retained some function. In our system, we did not detect any full-length or truncated Bis protein by Western blotting using three kinds of antibodies raised against whole, COOH-terminal, and NH_2-terminal Bis peptides (Fig. 1 and Supplemental Fig. S1). However, the possibility that the sensitivity of immunoblotting was not high enough to detect a tiny amount of truncated Bis protein in our assay, as well as in the previous model, cannot be excluded. Another possible explanation for the discrepancy in the reported phenotypes of *bis*-deficient mice may be the extent of homogeneity in the genetic background. Diverse genetic backgrounds in hybrid

Downloaded from ajpendo.physiology.org on January 18, 2009

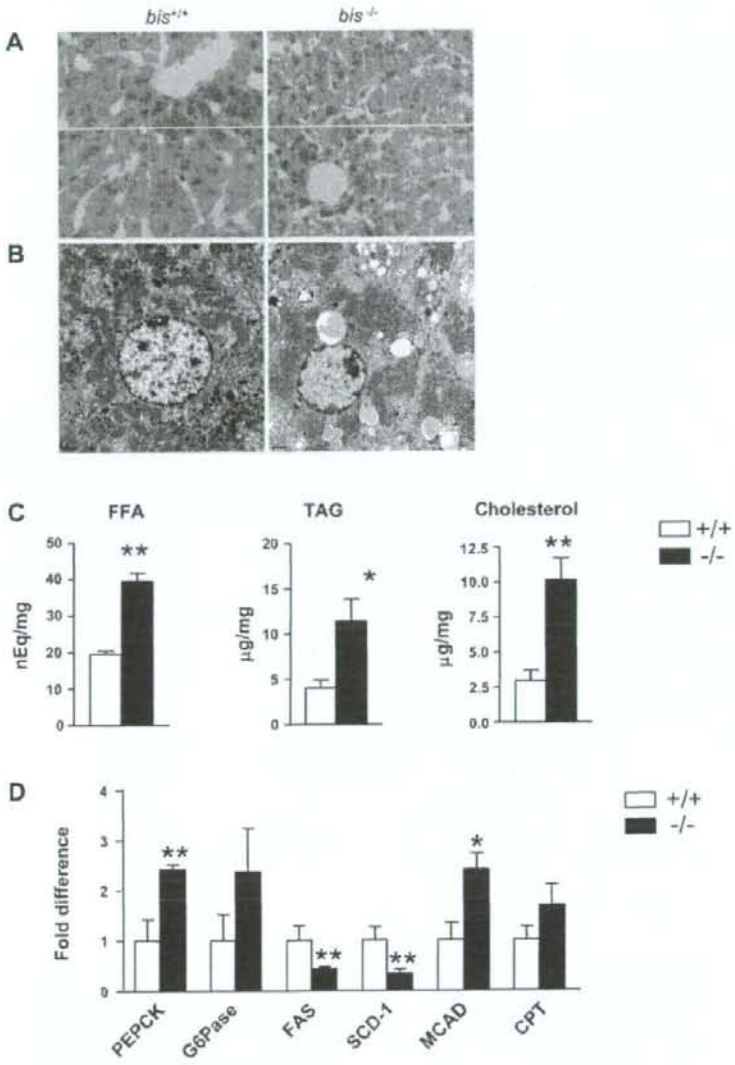

Fig. 3. Lipid accumulation in the liver of *bis*-deficient mice. *A*: Oil Red O staining of histological sections of liver from $bis^{+/+}$ and $bis^{-/-}$ mice. Red staining indicates neutral lipid accumulation. *B*: representative electron micrographs of $bis^{+/+}$ and $bis^{-/-}$ mice livers. Scale bars, 1 μm. *C*: increased levels of free fatty acid (FFA), triglyceride (TAG), and cholesterol in livers of $bis^{-/-}$ mice compared with livers of wild-type littermates. Results are expressed as means ± SE for 5 animals at 16 days of age. $*P < 0.05$, $**P < 0.01$, compared with wild-type littermates. *D*: alteration in mRNA levels of several genes involved in glucose or lipid metabolism in *bis*-deficient mice: quantitative RT-PCR of selected genes from livers of wild-type and *bis*-deficient mice. Data are means ± SE of 3 animals in each group, older than 15 days of age. Data are normalized relative to cyclophilin mRNA in the same samples, and wild-type values were arbitrarily set as 1.0. $*P < 0.05$, $**P < 0.01$, compared with wild-type littermates.

strains result in different degrees of compensatory responses, especially in response to metabolic challenges (2). For the generation of homozygous $bis^{-/-}$ mice we used heterozygous mice that were backcrossed with C57BL6 more than eight generations. Thus the effect of the Sv129 genetic background on the phenotypes of our study appeared insignificant. It is also possible that the metabolic disturbances observed in this study using biochemical and ultrastructure assays were not noticeable in the histological examinations performed by the previous research group.

The cause of death of the $bis^{-/-}$ mice was previously suggested to be respiratory failure, based on the marked degeneration of the diaphragm and intercostal muscle (10). It was also postulated that the decreased cardiac performance and subsequent pulmonary edema may have played a role in the death of the $bis^{-/-}$ mice (10). In the present study, massive apoptosis and degeneration of skeletal muscles were not observed in $bis^{-/-}$ mice (Fig. 4), suggesting that the loss of antiapoptotic activity in muscles is not the primary cause of death in these mice. Instead, the serious metabolic deterioration, such as sustained hypoglycemia and lipid accumulation in the liver, observed in our $bis^{-/-}$ mice model, may be ultimately responsible for the death of the animals.

What causes the perturbations in glucose and lipid metabolism in $bis^{-/-}$ mice? Analysis of the hepatic expression of key enzymes in the pathways of glucose and lipid metabolism

Downloaded from ajpendo.physiology.org on January 18, 2009

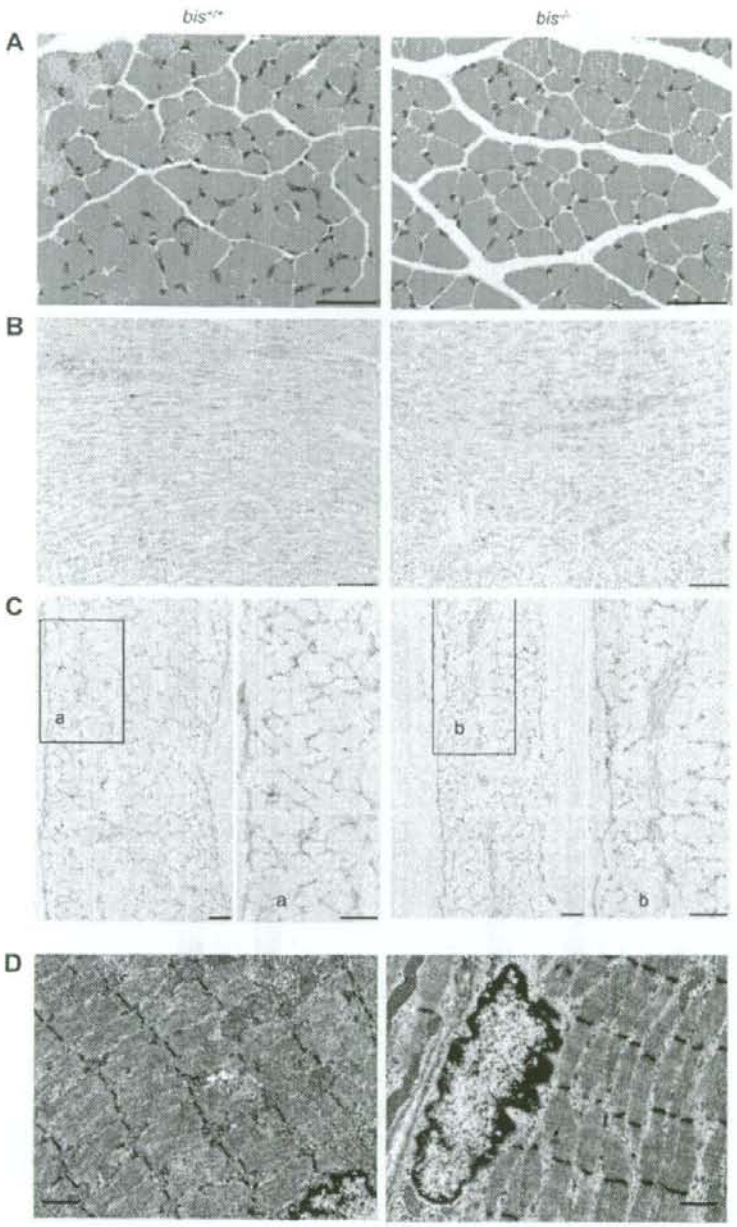

Fig. 4. No massive apoptotic features in myocytes of *bis*-deficient mice. *A*: hematoxylin and eosin staining of quadriceps femoris muscles of wild-type and *bis*-deficient mice. Scale bars, 30 μm. *B* and *C*: TUNEL staining of ventricle (*B*) and thin sections of diaphragm (*C*) of wild-type and $bis^{-/-}$ mice. *C*, *a* and *b*: Higher magnifications of boxed areas. Scale bars, 50 μm. *D*: transelectron microscopy of quadriceps femoris muscles of wild-type and *bis*-deficient mice. Scale bars, 1 μm.

revealed an increase in gluconeogenesis and lipolysis and a decrease in lipogenesis in $bis^{-/-}$ mice (Fig. 3*D*). These changes, which were also accompanied by a decrease in peripheral fat and serum triglyceride levels (Table 2), are typical of the adaptive response to a scarcity of glucose in serum that supplies the energy for gluconeogenesis in the liver, which is observed after fasting (35). Since we frequently observed that, even throughout their weight loss, $bis^{-/-}$ mice were trying to suckle, it is unlikely that isolation from the feeding mother or loss of appetite was the cause of their hypoglycemia. An impediment in the uptake or absorption of milk possibly caused delayed growth, due to an insufficiency

Downloaded from ajpendo.physiology.org on January 18, 2009

of nutrients for normal growth, and substantially metabolic deterioration, the same results of fasting. Since the amounts of milk in the stomachs of $bis^{-/-}$ mice were low at ≥16 days of age and no obvious histological abnormalities were found in the intestines of $bis^{-/-}$ mice (Supplemental Fig. S2), the ingestion of milk, rather than the process of absorption, appears to be impaired in $bis^{-/-}$ mice. The hypothesis that hypophagia or dysphagia is linked to nutritional problems and growth retardation in $bis^{-/-}$ mice is supported by a previous mutation study of *starvin* (*stv*), a *Drosophila* gene encoding a Bag-domain protein (6). The Bag domain is located in the COOH terminal of Bis, shared with several proteins comprising the Bag family (33). Coulson et al. (6) showed that mutation of *stv* results in a failure of larvae to grow after hatching and a severely impaired ability to take up food. The expression of STV was shown to be highly specific in embryonic somatic muscle and tendon cells, suggesting a role in muscle development or function. However, the gross morphology and function of somatic muscles including mouth-hook movement is predominantly normal in *stv* mutants, indicating that the feeding disability of *stv* mutants is not linked to dysfunction of skeletal muscles. Thus, in light of the study of *stv* mutants of *Drosophila*, the malnutrition status observed in *bis* deficiency is associated with impairment in uptake of milk, which is probably not caused by dysfunction of skeletal muscles. However, although obvious apoptotic changes were not found in the skeletal muscles in $bis^{-/-}$ mice, it is possible that Bis deletion caused functional weakness of muscles involved in suckling or swallowing or abnormal esophageal motor function shown in achalasia, a esophageal motility disorder in humans (16). Therefore, the role of Bis in the physiological regulation of swallowing remains to be elucidated.

We also observed a dramatic involution of the thymus and spleen in mice with a homozygous *bis* gene deletion (Fig. 2, *C* and *D*). At present, the direct link between the two representative phenotypes of $bis^{-/-}$ mice, metabolic deterioration and involution of the thymus and spleen, remains unclear. The thymus has been shown to be significantly affected in malnutrition, undergoing a severe atrophy due to apoptosis-induced thymocyte depletion (22, 24, 30). We showed that the reduction in the relative weight of the thymus and spleen was not obvious until 12 days after birth (Fig. 2*E*), at a time when body weight was still increasing and the serum glucose level was within the normal range (Fig. 2*A* and data not shown). Thus the involution of the thymus and spleen appears to be directly or indirectly linked to the nutritional status of $bis^{-/-}$ mice. Shrinkage of the thymus and spleen has also been described in *bcl-2*-deficient mice (13, 36). Since Bis binds Bcl-2 (18), interaction between Bis and Bcl-2 may be required for normal physiology of these lymphoid organs. However, $bcl\text{-}2^{-/-}$ mice have selective lymphopenia, but $bis^{-/-}$ mice have an overall decrease in white blood cells (Table 1). Furthermore, thymic and hepatic levels of Bcl-2 and HSP70, another Bis binding partner (33), were not decreased in protein extracts from *bis*-deficient mice in a Western blot analysis (data not shown). Thus the phenotypes observed in $bis^{-/-}$ mice are not mainly due to the disruption of the interaction between Bis and Bcl-2, or HSP70, but due to the specific effect of ablation of *bis* gene.

Bis has been shown to be highly expressed in lymphocytic leukemia cells, and downmodulation of Bis increases susceptibility to apoptosis in normal and neoplastic leukocytes (26–28). Therefore, our results showing significant decrease in leukocytes in peripheral blood cells from $bis^{-/-}$ mice support the previous reports for survival-sustaining roles of Bis in leukocytes. However, it is not certain whether the absence of Bis affects the viability of peripheral leukocytes or the function of progenitor cells in bone marrow. Thus, with the shrinkage of lymphoid organs, the decreases in the leukocyte numbers in $bis^{-/-}$ mice suggest the expanded roles of Bis in the physiology of hematopoietic cells and in the development of lymphoid organs, not confined to prosurvival activity of lymphocytes.

In this study, we generated *bis*-deficient mice and demonstrated that *bis* ablation resulted in growth retardation and early lethality with serious metabolic deterioration and involution of the thymus and spleen. Our results suggest that Bis is critical for postnatal growth and survival. However, the critical role for Bis in the regulation of feeding and the physiology of the thymus and spleen, which may or may not be linked, remains to be fully defined.

ACKNOWLEDGMENTS

We thank Y. Maruyama and A. Kawai for technical assistances and I. H. Oh and J. Kim for helpful discussions.

GRANTS

This work was partly supported by a Korea Research Foundation Grant funded by the Korean government (MOEHRD) (KRF-2004-041-E00043), a Korea Science and Engineering Foundation (KOSEF) grant funded by the Korean government (MOST) (R01-2006-000-10208-0), grants for Scientific Research from the Ministry of Education, Science, Sports and Culture, and a grant for Research on Dementia and Bone Fracture from the Ministry of Health, Labor and Welfare, Japan.

REFERENCES

1. **Bonelli P, Petrella A, Rosati A, Romano MF, Lerose R, Pagliuca MG, Amelio T, Festa M, Martire G, Venuta S, Turco MC, Leone A.** BAG3 protein regulates stress-induced apoptosis in normal and neoplastic leukocytes. *Leukemia* 18: 358–360, 2004.
2. **Burgess SC, Jeffrey FM, Storey C, Milde A, Hausler N, Merritt ME, Mulder H, Holm C, Sherry AD, Malloy CR.** Effect of murine strain on metabolic pathways of glucose production after brief or prolonged fasting. *Am J Physiol Endocrinol Metab* 289: E53–E61, 2005.
3. **Chakravarthy MV, Pan Z, Zhu Y, Tordjman K, Schneider JG, Coleman T, Turk J, Semenkovich CF.** "New" hepatic fat activates PPARalpha to maintain glucose, lipid, and cholesterol homeostasis. *Cell Metab* 1: 309–322, 2005.
4. **Chen L, Wu W, Dentchev T, Zeng Y, Wang J, Tsui I, Tobias JW, Bennett J, Baldwin D, Dunaief JL.** Light damage induced changes in mouse retinal gene expression. *Exp Eye Res* 79: 239–247, 2004.
5. **Chiappetta G, Ammirante M, Basile A, Rosati A, Festa M, Monaco M, Vuttariello E, Pasquinelli R, Arra C, Zerilli M, Todaro M, Stassi G, Pezzullo L, Gentilella A, Tosco A, Pascale M, Marzullo L, Belisario MA, Turco MC, Leone A.** The antiapoptotic protein BAG3 is expressed in thyroid carcinomas and modulates apoptosis mediated by tumor necrosis factor-related apoptosis-inducing ligand. *J Clin Endocrinol Metab* 92: 1159–1163, 2007.
6. **Coulson M, Robert S, Saint R.** *Drosophila* starvin encodes a tissue-specific BAG-domain protein required for larval food uptake. *Genetics* 171: 1799–1812, 2005.
7. **Doong H, Price J, Kim YS, Gasbarre C, Probst J, Liotta LA, Blanchette J, Rizzo K, Kohn E.** CAIR-1/BAG-3 forms an EGF-regulated ternary complex with phospholipase C-gamma and Hsp70/Hsc70. *Oncogene* 19: 4385–4395, 2000.
8. **Finck BN, Gropler MC, Chen Z, Leone TC, Croce MA, Harris TE, Lawrence JC Jr, Kelly DP.** Lipin 1 is an inducible amplifier of the hepatic PGC-1alpha/PPARalpha regulatory pathway. *Cell Metab* 4: 199–210, 2006.
9. **Foretz M, Ancellin N, Andreelli F, Saintillan Y, Grondin P, Kahn A, Thorens B, Vaulont S, Viollet B.** Short-term overexpression of a consti-

Downloaded from ajpendo.physiology.org on January 18, 2009

tutively active form of AMP-activated protein kinase in the liver leads to mild hypoglycemia and fatty liver. *Diabetes* 54: 1331–1339, 2005.

10. **Homma S, Iwasaki M, Shelton GD, Engvall E, Reed JC, Takayama S.** BAG3 deficiency results in fulminant myopathy and early lethality. *Am J Pathol* 169: 761–773, 2006.
11. **Inoue N, Ikawa M, Isotani A, Okabe M.** The immunoglobulin superfamily protein Izumo is required for sperm to fuse with eggs. *Nature* 434: 234–238, 2005.
12. **Iwasaki M, Homma S, Hishiya A, Dolezal SJ, Reed JC, Takayama S.** BAG3 regulates motility and adhesion of epithelial cancer cells. *Cancer Res* 67: 10252–10259, 2007.
13. **Kamada S, Shimono A, Shinto Y, Tsujimura T, Takahashi T, Noda T, Kitamura Y, Kondoh H, Tsujimoto Y.** bcl-2 deficiency in mice leads to pleiotropic abnormalities: accelerated lymphoid cell death in thymus and spleen, polycystic kidney, hair hypopigmentation, and distorted small intestine. *Cancer Res* 55: 354–359, 1995.
14. **Kassis JN, Guancial EA, Doong H, Virador V, Kohn EC.** CAIR-1/BAG-3 modulates cell adhesion and migration by downregulating activity of focal adhesion proteins. *Exp Cell Res* 312: 2962–2971, 2006.
15. **Kyratsous CA, Silverstein SJ.** BAG3, a host cochaperone, facilitates varicella-zoster virus replication. *J Virol* 81: 7491–7503, 2007.
16. **Lacy BE, Weiser K.** Esophageal motility disorders: medical therapy. *J Clin Gastroenterol* 42: 652–658, 2008.
17. **Lee JH, Jeon MH, Seo YJ, Lee YJ, Ko JH, Tsujimoto Y, Lee JH.** CA repeats in the 3′-untranslated region of bcl-2 mRNA mediate constitutive decay of bcl-2 mRNA. *J Biol Chem* 279: 42758–42764, 2004.
18. **Lee JH, Takahashi T, Yasuhara N, Inazawa J, Kamada S, Tsujimoto Y.** Bis, a Bcl-2-binding protein that synergizes with Bcl-2 in preventing cell death. *Oncogene* 18: 6183–6190, 1999.
19. **Lee MY, Kim SY, Choi JS, Choi YS, Jeon MH, Lee JH, Kim IK, Lee JH.** Induction of Bis, a Bcl-2-binding protein, in reactive astrocytes of the rat hippocampus following kainic acid-induced seizure. *Exp Mol Med* 34: 167–171, 2002.
20. **Lee MY, Kim SY, Shin SL, Choi YS, Lee JH, Tsujimoto Y, Lee JH.** Reactive astrocytes express bis, a bcl-2-binding protein, after transient forebrain ischemia. *Exp Neurol* 175: 338–346, 2002.
21. **Liao Q, Ozawa F, Friess H, Zimmermann A, Takayama S, Reed JC, Kleeff J, Buchler MW.** The anti-apoptotic protein BAG-3 is overexpressed in pancreatic cancer and induced by heat stress in pancreatic cancer cell lines. *FEBS Lett* 503: 151–157, 2001.
22. **Morishita S, Sato EF, Takahashi K, Manabe M, Inoue M.** Insulin-induced hypoglycemia elicits thymocyte apoptosis in the rat. *Diabetes Res Clin Pract* 40: 1–7, 1998.
23. **Pagliuca MG, Lerose R, Cigliano S, Leone A.** Regulation by heavy metals and temperature of the human BAG-3 gene, a modulator of Hsp70 activity. *FEBS Lett* 541: 11–15, 2003.
24. **Prentice AM.** The thymus: a barometer of malnutrition. *Br J Nutr* 81: 345–347, 1999.
25. **Proctor G, Jiang T, Iwahashi M, Wang Z, Li J, Levi M.** Regulation of renal fatty acid and cholesterol metabolism, inflammation, and fibrosis in Akita and OVE26 mice with type 1 diabetes. *Diabetes* 55: 2502–2509, 2006.
26. **Romano MF, Festa M, Pagliuca G, Lerose R, Bisogni R, Chiurazzi F, Storti G, Volpe S, Venuta S, Turco MC, Leone A.** BAG3 protein controls B-chronic lymphocytic leukaemia cell apoptosis. *Cell Death Differ* 10: 383–385, 2003.
27. **Romano MF, Festa M, Petrella A, Rosati A, Pascale M, Bisogni R, Poggi V, Kohn EC, Venuta S, Turco MC, Leone A.** BAG3 protein regulates cell survival in childhood acute lymphoblastic leukemia cells. *Cancer Biol Ther* 2: 508–510, 2003.
28. **Rosati A, Ammirante M, Gentilella A, Basile A, Festa M, Pascale M, Marzullo L, Belisario MA, Tosco A, Franceschelli S, Moltedo O, Pagliuca G, Lerose R, Turco MC.** Apoptosis inhibition in cancer cells: a novel molecular pathway that involves BAG3 protein. *Int J Biochem Cell Biol* 39: 1337–1342, 2007.
29. **Rosati A, Leone A, Del Valle L, Amini S, Khalili K, Turco MC.** Evidence for BAG3 modulation of HIV-1 gene transcription. *J Cell Physiol* 210: 676–683, 2007.
30. **Savino W, Dardenne M, Velloso LA, Dayse Silva-Barbosa S.** The thymus is a common target in malnutrition and infection. *Br J Nutr* 98, *Suppl* 1: S11–S16, 2007.
31. **Schwarz DA, Barry G, Mackay KB, Munu F, Naeve GS, Vana AM, Verge G, Conlon PJ, Foster AC, Maki RA.** Identification of differentially expressed genes induced by transient ischemic stroke. *Brain Res Mol Brain Res* 101: 12–22, 2002.
32. **Seo YJ, Jeon MH, Lee JH, Lee YJ, Youn HJ, Ko JH, Lee JH.** Bis induces growth inhibition and differentiation of HL-60 cells via up-regulation of p27. *Exp Mol Med* 37: 624–630, 2005.
33. **Takayama S, Xie Z, Reed JC.** An evolutionarily conserved family of Hsp70/Hsc70 molecular chaperone regulators. *J Biol Chem* 274: 781–786, 1999.
34. **Tanaka N, Moriya K, Kiyosawa K, Koike K, Gonzalez FJ, Aoyama T.** PPARalpha activation is essential for HCV core protein-induced hepatic steatosis and hepatocellular carcinoma in mice. *J Clin Invest* 118: 683–694, 2008.
35. **Teusink B, Voshol PJ, Dahlmans VE, Rensen PC, Pijl H, Romijn JA, Havekes LM.** Contribution of fatty acids released from lipolysis of plasma triglycerides to total plasma fatty acid flux and tissue-specific fatty acid uptake. *Diabetes* 52: 614–620, 2003.
36. **Veis DJ, Sorenson CM, Shutter JR, Korsmeyer SJ.** Bcl-2-deficient mice demonstrate fulminant lymphoid apoptosis, polycystic kidneys, and hypopigmented hair. *Cell* 75: 229–240, 1993.

Downloaded from ajpendo.physiology.org on January 18, 2009

Supplemental Material can be found at:
http://www.jbc.org/cgi/content/full/M708590200/DC1

THE JOURNAL OF BIOLOGICAL CHEMISTRY VOL. 283, NO. 27, pp. 19039–19048, July 4, 2008
© 2008 by The American Society for Biochemistry and Molecular Biology, Inc. Printed in the U.S.A.

Meichroacidin Containing the Membrane Occupation and Recognition Nexus Motif Is Essential for Spermatozoa Morphogenesis*[S]

Received for publication, October 16, 2007, and in revised form, April 29, 2008 Published, JBC Papers in Press, May 3, 2008, DOI 10.1074/jbc.M708590200

Keizo Tokuhiro[‡§], Mika Hirose[‡§], Yasushi Miyagawa[¶], Akira Tsujimura[¶], Shinji Irie[‖], Ayako Isotani[§], Masaru Okabe[§], Yoshiro Toyama[**], Chizuru Ito[**], Kiyotaka Toshimori[**], Ken Takeda[‡‡], Shigeru Oshio[‡‡], Hitoshi Tainaka[‡], Junji Tsuchida[§1], Akihiko Okuyama[¶], Yoshitake Nishimune[§§], and Hiromitsu Tanaka[‡§2]

From the [‡]TANAKA Project, Center for Advanced Science and Innovation, Osaka University, 3-1 Yamadaoka, Suita, Osaka 565-0871, [§]Animal Resource Center for Infectious Diseases, Research Institute for Microbial Diseases, Osaka University, 3-1 Yamadaoka, Suita, Osaka 565-0871, the [¶]Department of Urology, Osaka University Graduate School of Medicine, 3-1 Yamadaoka, Suita, Osaka 565-0871, [‖]Life Science Department, Business Incubation Center, Corporate Manufacturing, Technology, and Research Division, Toppan Printing Company, Ltd., 1-3-3 Suido, Bunkyo-ku, Tokyo 112-8531, the [**]Department of Anatomy and Developmental Biology, Graduate School of Medicine, Chiba University, Chiba 260-8670, the [‡‡]Department of Hygiene Chemistry, Faculty of Pharmaceutical Sciences, Tokyo University of Science, Chiba 278-8510, and [§§]Research Collaboration Center on Emerging and Re-emerging Infections, Research Institute for Microbial Diseases, Osaka University, 3-1 Yamadaoka, Suita, Osaka 565-0871, Japan

Meichroacidin (MCA) is a highly hydrophilic protein that contains the membrane occupation and recognition nexus motif. MCA is expressed during the stages of spermatogenesis from pachytene spermatocytes to mature sperm development and is localized in the male meiotic metaphase chromosome and sperm flagellum. *MCA* sequences are highly conserved in *Ciona intestinalis*, *Cyprinus carpio*, and mammals. To investigate the physiological role of MCA, we generated *MCA*-disrupted mutant mice; homozygous *MCA* mutant males were infertile, but females were not. Sperm was rarely observed in the caput epididymidis of *MCA* mutant males. However, little to no difference was seen in testis mass between wild-type and mutant mice. During sperm morphogenesis, elongated spermatids had retarded flagellum formation and might increase phagocytosis by Sertoli cells. Immunohistochemical analysis revealed that MCA interacts with proteins located on the outer dense fibers of the flagellum. The testicular sperm of *MCA* mutant mice was capable of fertilizing eggs successfully via intracytoplasmic sperm injection and generated healthy progeny. Our results suggest that MCA is essential for sperm flagellum formation and the production of functional sperm.

Haploid cells differentiate only during spermiogenesis following meiosis. The specific features of spermiogenesis include the formation of the tail, mitochondria, and acrosome, nuclear condensation, and the elimination of spermatid cytoplasm. To understand haploid germ cell differentiation fully, *i.e.* spermiogenesis, it is important to identify and characterize specific genes expressed during these developmental processes (1). Meichroacidin (MCA,[3] male meiotic metaphase chromosome-associated acidic protein) was originally isolated using polyclonal antibodies against testicular antigens (2) and is expressed in male germ cells and expressed weakly in the mouse ovary. Specifically, MCA protein is localized predominantly in the cytoplasm of cells throughout the stages of sperm development, *i.e.* from pachytene spermatocytes to round spermatids, as well as in the regions of metaphase chromosomes and spindles during both the first and second meiotic divisions (2). The amino acid sequence of MCA contains a set of seven nominal repeat sequences consisting of the repeat sequence *YXGXX(X)XXXX*-HGQG (2). Recently, junctophilins (JPs), which are a novel conserved family of proteins that are components of the junctional complexes, were reported to contain a repeat amino acid sequence similar to that of MCA (3). However, MCA consists of a hydrophilic amino acid region, whereas JPs have a C-terminal hydrophobic segment spanning the endoplasmic/sarcoplasmic reticulum and are expressed abundantly in a variety of tissues (3, 4). The repeat amino acid sequence, referred to as the membrane occupation and recognition nexus (MORN) motif, is a novel protein-folding module that is shared by functionally different proteins and may have specific physiological roles (3). Southern blots revealed positive bands hybridizing to mouse

* This work was supported in part by grants received from Research and Development to Promote the Creation and Utilization of an Intellectual Infrastructure by the New Energy and Industrial Technology Development Organization of Japan and by the Ministry of Education, Culture, Sports, Science, and Technology of Japan. The costs of publication of this article were defrayed in part by the payment of page charges. This article must therefore be hereby marked "*advertisement*" in accordance with 18 U.S.C. Section 1734 solely to indicate this fact.

[S] The on-line version of this article (available at http://www.jbc.org) contains supplemental Figs. S1–S7 and Tables S1 and S2.

[1] Present address: Dept. of Patho-histocytochemistry, Discovery Research Technologies, Discovery Research Laboratories, Shionogi and Co., Ltd., Sagisu 5-12-4, Fukushima-ku, Osaka 553-0022, Japan.

[2] To whom correspondence should be addressed: Faculty of Pharmaceutical Sciences, Nagasaki International University, Huis Ten Bosch, Sasebo, Nagasaki 859-3298, Japan. Tel./Fax: 81-956-20-5651; E-mail: h-tanaka@niu.ac.jp.

[3] The abbreviations used are: MCA, meichroacidin; MORN, membrane occupation and recognition nexus; JP, junctophilin; SNP, single nucleotide polymorphism; ODF, outer dense fiber; TUNEL, deoxynucleotidyltransferase-mediated dUTP nick end-labeling; PBS, phosphate-buffered saline; FITC, fluorescein isothiocyanate; CTAB, cetyltrimethylammonium bromide; PFA, paraformaldehyde; FS/H, fibrous sheath/head; h, human; Ax, axoneme.

ASBMB The Journal of Biological Chemistry jbc

Downloaded from www.jbc.org at OSAKA UNIVERSITY on January 18, 2009

MCA cDNA probes in chromosomal DNA samples from other species, including rats, chickens, *Xenopus*, pufferfish, and humans (2). Recently, the *MCA* homolog of the carp (*Cyprinus carpio*) MORN motif-containing sperm-specific axonemal protein (MSAP) was cloned and characterized (5). *MCA* homologs have been found in organisms ranging from unicellular green algae to mammals through the use of computer-assisted analysis (5). In carp and ascidians (*Ciona intestinalis*), *MSAP* is expressed during late spermatogenesis and accumulates in mature spermatozoa, where it is localized in the basal body and flagellum (5, 6). The isolation and characterization of human *MCA* (*h-MCA*) indicate that h-MCA protein is localized in the sperm flagellum and basal body (7, 8). These results suggest that h-MCA plays an important physiological role in flagellum formation during spermiogenesis.

Here we demonstrated that MCA is expressed in cytoplasm spermatids and is dominantly localized in the outer dense fibers of the flagellum. In addition, mice deficient in MCA exhibit male infertility and azoospermia because of impaired sperm formation. We used single nucleotide polymorphism (SNP) studies to identify two SNPs that induce amino acid substitutions in azoospermic or oligospermic infertile human males. It is possible that SNPs in MCA are related to human infertility.

EXPERIMENTAL PROCEDURES

Animals—All mice were bred and maintained in our laboratory animal facilities and used in accordance with the guidelines for the care and use of laboratory animals set forth by the Japanese Association for Laboratory Animal Science. The mice were kept under controlled temperature and lighting conditions throughout the experiments and were provided with food and water *ad libitum*.

Northern Blots—Total RNA was isolated from various mouse tissues using RNA zolTM B (Invitrogen). Total RNA was extracted according to the manufacturer's instructions and was quantified using optical density measurements. RNA samples containing 2.2 M formaldehyde were electrophoresed in 1.1% agarose gels containing 0.66 M formaldehyde. The RNA was transferred to a nitrocellulose filter in 20× SSC and hybridized with ^{32}P-labeled cDNA prepared using the BcaBest random primer kit (Takara, Shiga, Japan) at 65 °C for 2 h in a PerfectHyb (Toyobo, Osaka, Japan).

Western Blots—Testes freshly removed from mice were homogenized on ice with TBS-T buffer (100 mmol/liter Tris-HCl, pH 7.5, 150 mmol/liter NaCl, 0.2% Tween 20). After centrifugation at 17,800 × *g*, the protein concentration of the supernatant was estimated using a Bradford protein assay (Nacalai, Kyoto, Japan). Following protein quantification, 50 μg of protein from each extract were subjected to SDS-PAGE, followed by electroblotting to a polyvinylidene difluoride membrane (Millipore, Bedford, MA). The membranes were blocked with 5% nonfat dry milk and washed for 15 min with TBS (100 mmol/liter Tris-HCl, pH 7.5, 150 mmol/liter NaCl). They were then incubated with each antibody overnight at 4 °C and washed in TBS once for 3 min and then three times for 5 min each. Finally, the membranes were incubated with peroxidase-conjugated anti-rat or anti-rabbit immunoglobulins (1:500; Amersham Biosciences) for 2 h at 25 °C. After further washing, the reactive bands were visualized on development with the POD staining kit (Wako, Osaka, Japan).

Immunoprecipitation—Testicular fractions were lysed with RIPA (10 mmol/liter Tris-HCl, pH 7.5, 150 mmol/liter NaCl, 0.1% deoxycholic acid, 0.3% SDS, 1% Nonidet P-40, and 0.5 ml/liter protease inhibitor mixture; Nacalai). Each antibody was added to Dynabeads-protein G (Invitrogen), washed once with PBS, and then washed three times with PBS containing 0.01% Tween 20 as per the manufacturer's recommendations. The lysates were then centrifuged at 10,000 rpm for 10 min at 4 °C. Glycerol was added to the supernatants at a concentration of 10%. The Dynabeads-protein G was treated with the lysates at 4 °C overnight and was then washed with PBS containing 10% glycerol and 0.1% Tween 20. SDS sample buffer was added to the Dynabeads-protein G, and each sample was subjected to Western blotting.

Mouse Sperm Protein Fractionation—Sperm was collected from 10 mice using Percoll (9) and was fractionated according to a previously described adapted protocol (10). Briefly, sperm was washed from the epididymis and vas deferens and subjected to three sequential extractions at 4 °C in 500 μl of a solution containing 1% Triton X-100 and 2 mM dithiothreitol in 50 mM sodium borate buffer at pH 9.0 for 40 min each. After each extraction, the samples were centrifuged at 400 × *g* using a Tomy MRX-150 centrifuge (Tomy, Tokyo, Japan), and the supernatants were collected (membrane soluble fractions: M1, M2, and M3). The pellet was washed three times with 50 mM sodium borate buffer and suspended in 500 μl of a solution of 0.6 M potassium thiocyanate (KSCN), 2 mM dithiothreitol, and 50 mM Tris-HCl, pH 8.0, for 2 h at 4 °C. After centrifugation at 800 × *g*, the supernatant was collected (central axoneme (Ax) fraction), and the pellet was extracted overnight at 4 °C in 500 μl of a solution containing 4 M urea, 50 mM Tris-HCl, pH 8.0, and 2 mM dithiothreitol. A final centrifugation at 17,800 × *g* was performed to separate the urea-extracted fraction (urea fraction, ODF). Finally, the resulting nonextracted pellet was washed in borate buffer three times, suspended in sperm extraction buffer (62.5 mM Tris-HCl, pH 6.8, 2% SDS, 10% glycerol, and 5% mercaptoethanol), and sonicated on ice for 10 min (fibrous sheath/head fraction: FS/H). The protein concentration of each fraction (*i.e.* M1, M2, M3, Ax, ODF, and FS/H) was estimated using the Bradford protein assay (Nacalai). Fractions M3, Ax, and ODF were precipitated with 10% trichloroacetic acid. Approximately 20 μg of protein from each fraction was separated by SDS-PAGE in 10% polyacrylamide gels. Western blotting was performed as described above. Control antibodies for the membrane (anti-Izumo1) (11), FS/H (anti-AKAP82) (12), and ODF (anti-Odf1) fractions (13) at a final dilution of 500× were used to verify the extracted proteins.

Immunohistochemistry of Sperm—Mouse sperm from the vas deferens and caudal epididymis suspended in PBS was filtered through a nylon mesh and centrifuged at 400 × *g*. The pellet was then washed in PBS, and a few drops were placed on glass slides and dried at 55 °C for 10 min. The slides were blocked with 10% blocking solution (Nacalai) whole serum in PBS for 30 min at room temperature. The drying and blocking conditions were kept the same for all immunohistochemical procedures. Blocked samples were incubated with anti-MCA antibodies (10

ASBMB The Journal of Biological Chemistry

Downloaded from www.jbc.org at OSAKA UNIVERSITY on January 18, 2009

μg/μl IgG) or preimmune serum IgG, both diluted in PBS (1000×), overnight at 4 °C. After one wash, the slides were treated with diluted (1000×) anti-rabbit IgG goat serum conjugated with rhodamine or fluorescein isothiocyanate (FITC) for 1 h at room temperature. The slides were then washed and examined under a fluorescence microscope. Triton X-100- and urea-treated sperm obtained from the fractionation of sperm proteins were also examined immunohistochemically using the same protocol. To visualize individual fibers of the ODF, mature sperm was treated for 1 h at room temperature with a solution containing 10 mM Tris-HCl, 30 mM β-mercaptoethanol, 0.2 mM phenylmethylsulfonyl fluoride, and 0.05% cetyltrimethylammonium bromide (CTAB), which is a cationic detergent that, under reducing conditions, extracts all tail structures except for the Odfs, which are released from the tight native form (14). Co-localization of MCA with Odf2 protein was accomplished by incubating intact and CTAB-treated sperm with anti-MCA antibodies that had been conjugated to rhodamine with an EZ-label rhodamine protein labeling kit (Pierce) for 1 h at room temperature. After a thorough wash in PBS, the samples were incubated with anti-Odf2 rabbit polyclonal antibodies for 2 h at room temperature, washed in PBS, and treated with FITC-conjugated diluted rabbit IgG antibody (2000×) for 1 h at room temperature.

Generation of MCA Targeting Mouse—The *MCA*-targeting construct was created by PCR amplification of a homologous 4-kb 5′ arm and 1-kb 3′ arm using *129Sv* genomic DNA as the template. Targeting at the *MCA* genomic locus resulted in the replacement of exons 1–3 with a neomycin cassette. Two amplified fragments were ligated sequentially into cloning sites on either side of the neomycin resistance gene in the targeting vector backbone. The targeting vector contained the neomycin resistance gene and a thymidine kinase gene, both under the control of the PGK promoter. The vector plasmid was linearized by NotI digestion before electroporation into W9.5 embryonic stem cells. Of 144 G418 gancyclovir-resistant clones that were screened for the targeting event, Southern blotting showed that two had undergone the correct homologous recombination. The two targeted cell lines were injected into C57BL/6J blastocysts, resulting in the birth of male chimeric mice. Highly chimeric males were mated with C57BL/6J wild-type females to generate F_1 offspring, half of which were heterozygous for the targeted allele. The embryonic stem cell lines were injected and produced a high percentage of chimeras that entered the germ line. Heterozygous F_1 males were then crossed with C57BL/6J females to obtain heterozygous F_2 animals. Heterozygous F_2 animals were bred to obtain homozygous mutants or to check the Mendelian inheritance. Eight mice older than 3 months were used to determine the fertility rate. The phenotypic variation was assessed, and biochemical analyses were conducted on samples from at least six individuals.

Southern Blotting and PCR—Genomic DNA was extracted from mouse tails using standard protocols (15). Southern blots were conducted to determine the site of the integration of the gene trap sequence in the *MCA* gene locus and to genotype the mice. A 700-bp probe for genomic Southern blotting was generated by PCR amplification from mouse genomic DNA. Genomic DNA samples (10 μg) were digested with ScaI and electrophoresed in 0.8% agarose gels. Southern hybridizations were carried out using standard protocols (15). The mice were genotyped by PCR using two sets of primers (see supplemental Fig. S1) as follows: one set of primers (5′-GGAGTAGCAAGTGATGTCAGGTCC-3′ and 5′-GAGTAACCTGAGGCTATGGCAGG-3′) to amplify the *Neo* gene and one set of primers (5′-CTATCAAGCAGTTACCAGCCACCC-3′ and 5′-GCAGAGGGAGCGAGGCTCAGCACATGG-3′) for the *MCA* gene.

Morphological and Immunohistochemical Observations—For the histochemical examination, fresh testis samples were embedded in O.T.C. compound embedding medium (Sakura Finetek, Tokyo, Japan) and frozen at −20 °C. Then 8-μm thick sections were prepared using a cryomicrotome (HM 500 OM; Microm, Walldorf, Germany) and fixed with 4% paraformaldehyde (PFA) at 4 °C for 10 min. Alternatively, testis samples were fixed in Bouin's solution for 24 h. After fixation, the samples were embedded in paraffin and sectioned at 8-μm thickness. Deparaffinized sections and frozen sections were incubated with the anti-MCA antibody (10 μg/μl IgG) or preimmune serum IgG, both diluted in PBS (1000×) overnight at 4 °C. After one wash, the slides were treated with diluted (1000×) anti-rabbit IgG goat serum conjugated with horseradish peroxidase for 1 h at room temperature. The slides were then washed and visualized by development with the POD immunostain kit (Wako, Osaka, Japan). Sections were treated with each antibody or stained with hematoxylin and eosin. Morphological identification of spermatogenic cells was based on the criteria of Russell *et al.* (16). The number of seminiferous tubules that sloughed spermatocytes or spermatids into the lumen was counted for 35 tubules of heterozygous or homozygous mutant mice.

For electron microscopy, the testis was perfused with 3% glutaraldehyde in HEPES buffer (10 mM HEPES and 145 mM NaCl). After post-fixation with 1% osmium tetroxide, the testis was embedded in Epon. Selected areas were then sectioned and examined.

Detection of Apoptosis—To identify apoptotic cells, we performed immunostaining with anti-active caspase 3 antibody (Promega, Madison, WI) and terminal deoxynucleotidyltransferase-mediated dUTP nick end-labeling (TUNEL) staining using an *in situ* apoptosis detection kit (Takara) according to the manufacturer's instructions. The number of TUNEL-positive signals was counted for 20 seminiferous tubules of heterozygous or homozygous mutant mice. To identify Sertoli cells, we used anti-GATA 4 antibody (Santa Cruz Biotechnology, Santa Cruz, CA). For immunostaining by anti-active caspase 3 and GATA 4, sections of testis fixed in 4% PFA were treated with an antigen unmasking solution (Vector Laboratories, Burlingame, CA). Immunostaining was performed according to the manufacturer's instructions.

Testicular Sperm Extraction with Intracytoplasmic Sperm Injection (TESE-ICSI)—Testis was placed in cold HEPES-CZB, and the tunica albuginea was removed. The bundles of seminiferous tubules were carefully separated using forceps. The separated tubules were examined under a dissecting microscope. Mature sperm was squeezed out from regions of the tubules that were darkened in the innermost part using forceps (17, 18).

The Journal of Biological Chemistry ASBMB

Downloaded from www.jbc.org at OSAKA UNIVERSITY on January 18, 2009

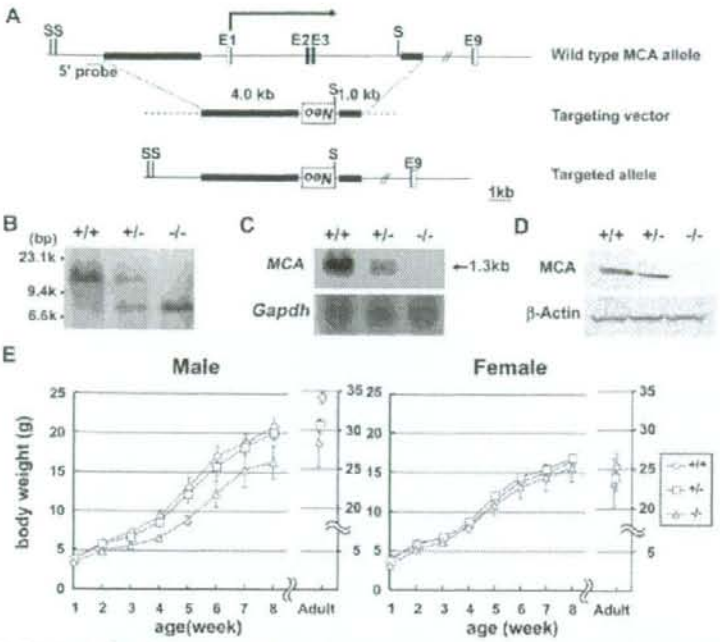

FIGURE 1. **Generation of *MCA* knock-out mice.** *A*, schematic representation of the methods used for gene targeting of the *MCA* genome. The gene targeting construct contains the *Neo* gene (*open box*) between the 4-kb 5′ arm and the 1-kb 3′ arm (*thick lines*). As a result, the regions of exons 1–3 were replaced by the *Neo* gene. Exon 1 includes the first methionine. *Arrows* indicate the transcriptional direction of *MCA*. *S* indicates ScaI restriction sites. *B*, targeted allele was identified by Southern blotting of genomic DNA digested with ScaI using a DNA probe created from the 5′ fragment. *C*, Northern blotting to localize gene expression. *MCA* transcripts are not detectable in the testis of *MCA* homozygous mice. The same membrane was re-hybridized with *Gapdh* cDNA as a control. *D*, Western blotting of testicular lysates of adult mice using an anti-MCA polyclonal antibody. The MCA protein is not detected in the testicular lysate of the homozygous mouse. β-Actin was used as a control. *E*, growth curve of male and female offspring from heterozygous matings (male $+/+$, $n = 4$; male $+/-$, $n = 9$; male $-/-$; $n = 4$; female $+/+$ l $n = 7$; male $+/-$, $n = 11$; female $-/-$, $n = 7$).

The sperm was suspended in 12% polyvinyl pyrrolidone in HEPES-CZB and injected into the cytoplasm of unfertilized eggs using a piezo-driven micromanipulator (Prime Tech, Ibaraki, Japan) within 1 h of preparation (19, 20). The injected eggs were cultivated in kSOM (20) overnight and then transferred to the oviducts of pseudopregnant females.

Serum Testosterone—Serum testosterone was measured using an enzyme immunoassay (testosterone enzyme-linked immunosorbent assay kit, catalog number 1880, Alpha Diagnostics, San Antonio, TX).

Identification of SNPs in the Open Reading Frame of MCA—Infertile patients ($n = 245$) were divided into subgroups according to the degree of defective spermatogenesis (21). Of these patients, 153 (68%) had nonobstructive azoospermia and 73 (32%) had severe oligospermia ($<5 \times 10^6$ cells/ml). The control group of fertile males ($n = 172$) included men who had fathered children born at the maternity clinic. DNA samples were extracted from the blood leukocytes of the infertile and proven-fertile males. Genomic DNA was isolated from the blood samples using protease and phenol purification (15). Eight PCR primer sets were designed to amplify the exons of *MCA* genes (see supplemental Tables S1 and S2 and supplemental Fig. S2). PCR was performed using PrimeSTAR or EX Taq hot start (Takara) (see supplemental Table S2). The PCR-amplified fragments were purified using CleanSEQ (Beckman Coulter, Tokyo, Japan), and thermal cycle sequencing (Applied Biosystems, Foster City, CA) was performed. The DNA sequences were determined using the same PCR primers.

Statistical Analysis—Differences between the experimental and control conditions were compared using one-way analysis of variance with Fisher's protected least significant difference tests. Significant differences ($p < 0.05$) are discussed.

RESULTS

MCA Homozygous Mutant Males Are Azoospermic—To investigate the physiological role of MCA, we generated homozygous *MCA* knock-out mice. We constructed the targeting vector (Fig. 1*A*), and homologous recombination was used to generate embryonic stem cell clones that were heterozygous for the *MCA* mutation. To produce chimeric mice, transgenic embryonic stem cells were injected into blastocysts that were subsequently implanted into pseudopregnant mice. We performed Southern blotting to confirm correct recombination (Fig. 1*B*). *MCA* mRNA was not detectable using Northern blots (Fig. 1*C*), and the 40-kDa MCA protein was not detectable using Western blots (Fig. 1*D*) of the testis of homozygous *MCA* mutant mice. Crosses of heterozygous mutant pairs produced the expected ratios of wild-type, heterozygous, and homozygous genotype offspring, according to classical Mendelian inheritance patterns. Homozygous mutant males had slightly smaller body masses than did wild-type males (Fig. 1*E*). Matings between homozygous *MCA* knock-out males and wild-type females did not produce any successful pregnancies during a period of more than 3 months of continuous cohabitation, although vaginal plugs were observed in the paired wild-type females (Table 1). The heterozygous male *MCA* mutant mice and the homozygous females were all fertile (Table 1). Female body mass (Fig. 1*E*), newborn pup growth rates (Fig. 1*E*), and the weights of various organs, including the testes and seminal vesicles of adult *MCA* homozygous mutant mice, did not differ significantly from those of wild-type mice (Table 2). The serum testosterone levels of adult *MCA* homozygous mutant mice were normal compared with those of wild-type mice (Table 2).

MCA Is Essential in Sperm Formation—To confirm the inactivation of *MCA*, an immunohistochemical examination was

ASBMB The Journal of Biological Chemistry

Downloaded from www.jbc.org at OSAKA UNIVERSITY on January 18, 2009

TABLE 1
Fertility rates of mutant mice

Genotype	Male fertility (no. of fertile males/no. of vaginal plugs)	Litter size (average no. of newborn pups)[a]	Female fertility (no. of fertile females/no. of vaginal plugs)	Litter size (average no. of newborn pups)[a]
−/−	10/10	8.2 ± 0.3	10/10	7.8 ± 0.3
−/−	0/21	0	8/8	6.0 ± 0.4

[a] Values are means ± S.E.

TABLE 2
Weights of organs, serum testosterone levels, and characteristics of seminiferous tubules in mutant mice
All values are means ± S.E. $n = 6$ mice per genotype.

Parameter	Value for $MCA^{-/-}$ mice	Value for $MCA^{+/-}$ mice	Value for $MCA^{+/+}$ mice
Wet weight of organs/body weight			
Testis	3.3 ± 0.2	3.5 ± 0.2	2.9 ± 0.2
Epididymis	1.5 ± 0.2	1.6 ± 0.1	1.5 ± 0.1
Seminal vesicle	12.7 ± 1.23	12.66 ± 1.45	13.47 ± 1.45
Testosterone level (ng/ml)	1.025 ± 0.730	1.305 ± 1.078	0.917 ± 0.622
Diameter of seminiferous tubules (μm, $n = 8$ tubules per genotype)	165.19 ± 5.82	168.83 ± 4.75	177.14 ± 4.33
No. of cells in seminiferous tubules ($n = 8$ tubules per genotype)	407.8 ± 15.6	421.5 ± 21.6	423.8 ± 15.9

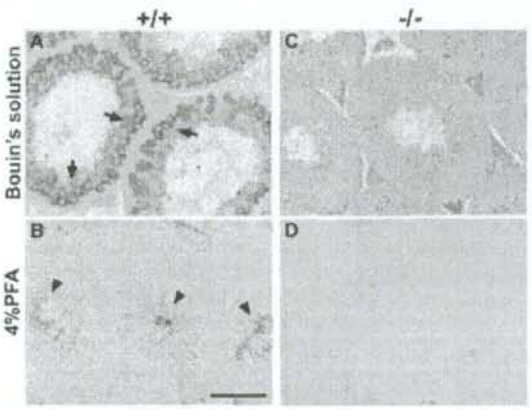

FIGURE 2. **Immunohistochemical staining of the cross-sections of mouse testis with anti-MCA antibody.** The cross-sections fixed in each solution (*left margin*) were incubated with anti-MCA antibody. Cross-sections of wild-type testis (*A* and *B*) or mutant testis (*C* and *D*) are shown. The signals of the cytoplasm of spermatocytes (*arrow*) (*A*) and sperm flagellum (*arrowheads*) (*B*) disappeared in cross-sections of mutant mice (*C* and *D*). *Bar* = 100 μm.

performed. The anti-MCA polyclonal antibody stained some germ cells in testis preserved in Bouin's solution (Fig. 2*A*) (2). The signal was detected in the spermatocytes and elongated spermatids (Fig. 2*A*), and these signals decreased gradually as morphogenesis proceeded, as reported by Tsuchida *et al.* (2). The heat treatment during embedding with paraffin or chemical bonds with the fixative solutions may have altered the exposed sites of the proteins to which the antibodies bound and may have caused the difference in immune staining. To examine the expression of MCA precisely, we performed immunohistochemical analyses using cross-sections preserved in 4% PFA (Fig. 2*B*). The anti-MCA antibody predominantly stained flagella in sperm preserved in 4% PFA (Fig. 2*B*). In *MCA* homozygous mutant males, the signals from testis preserved in either Bouin's solution or 4% PFA disappeared (Fig. 2, *C* and *D*). Rabbit IgG antibody was used as a control (see supplemental Fig. S3). These results indicate that the signals with both types of fixation depend on the *MCA* gene products. In addition, MCA was expressed from the pachytene spermatocyte (stage V) to sperm stages. These observations are in agreement with previous expression profile analyses using Northern and Western blotting (2). MCA might change the conformation in each subcellular localization and play different roles in sperm flagella and the cytoplasm of spermatocytes and spermatids; thus, the difference in conformation might cause different signals for each fixation method.

On microscopic examination, the diameter of the seminiferous tubules and number of cells within the testes of adult wild-type and *MCA* homozygous mutant mice did not differ significantly (Table 2). There were also no significant differences in testis mass between mutant and wild-type mice (Table 2). The spermatogonia, spermatocytes, and spermatids were arranged systematically in the seminiferous tubules in heterozygous mutant testes, just as in wild-type testes; the spermatogonia are located in the tubule walls, and the spermatids are located at the tubule centers, and spermatocytes are located between the two (Fig. 3, *A* and *B*). In mice, the spermatogenic cycle that occurs in each tubule of the seminiferous epithelium is divided into 12 stages (16). In addition, germ cells in the seminiferous tubules are enclosed by Sertoli cells. The spermatocytes or round spermatids had peeled from the Sertoli cells and were found at the tubule centers in ~6% of the seminiferous tubules of mutant testes. Therefore, the arrangement of germ cells in cross-sections was disturbed in *MCA* homozygous mutant testis tubules compared with *MCA* heterozygous mutant testis and wild-type tubules (Fig. 3, *E* and *F*). The epididymides of heterozygous mutant mice were filled with sperm (Fig. 3, *G* and *I*), whereas sperm were sparse or absent in the epididymides of homozygous mutant mice, as observed using light microscopy (Fig. 3, *H* and *J*). *MCA* mutant sperm that was present in the testes had few abnormalities and almost normal head shapes (Fig. 3, *K–P*).

Using electron microscopy, almost all sperm in homozygous *MCA* mutant testes showed abnormalities (Fig. 4 and supplemental Fig. S4), although developed sperm was observed in the seminiferous tubules using light microscopy, and there was no difference in the weights of mutant and wild-type testes (Fig. 3*D* and Table 2). Electron microscopy showed that most spermatids developed normally to step 9 in homozygous mutants (data not shown). However, following nuclear condensation, the rearrangement of mitochondria, and flagellum formation, we observed that the construction of these parts was disturbed, and small vacuoles appeared during spermatid elongation (Fig. 4*A*). Furthermore, the elongated spermatids in homozygous mutant testis were phagocytosed by Sertoli cells (Fig. 4*B* and supple-

ASBMB The Journal of Biological Chemistry

Downloaded from www.jbc.org at OSAKA UNIVERSITY on January 18, 2009

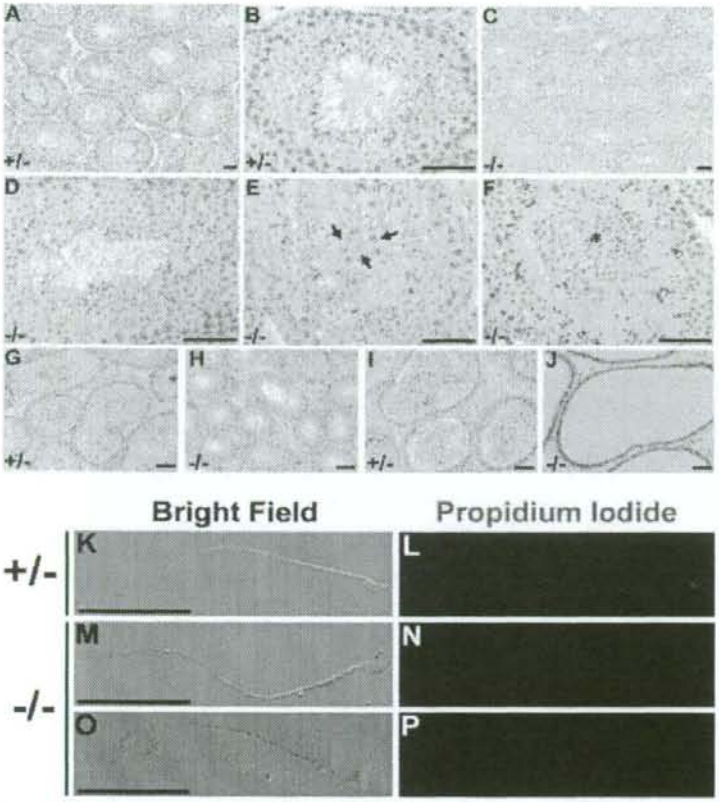

FIGURE 3. **Histological analyses of mutant testis, epididymides, and testicular sperm.** Cross-sections of heterozygous (*A* and *B*) or homozygous mutant (*C–F*) testis are shown. *B* and *D–F* show testicular tubules under high magnification. *Arrows* and an *asterisk* indicate irregularly arranged spermatocytes and round spermatids, respectively. Cross-sections of heterozygous (*G* and *I*) or homozygous mutant (*H* and *J*) epididymides are shown. *G* and *H* show caput epididymides and *I* and *J* show cauda epididymides. Sperm was not found in homozygous mutant epididymides (*H* and *J*). Heterozygous (*K* and *L*) and homozygous mutant (*M–P*) testicular sperm were observed. The heads of the homozygous mutant sperm have some abnormal features (*O* and *P*). *Bar* = 50 μm.

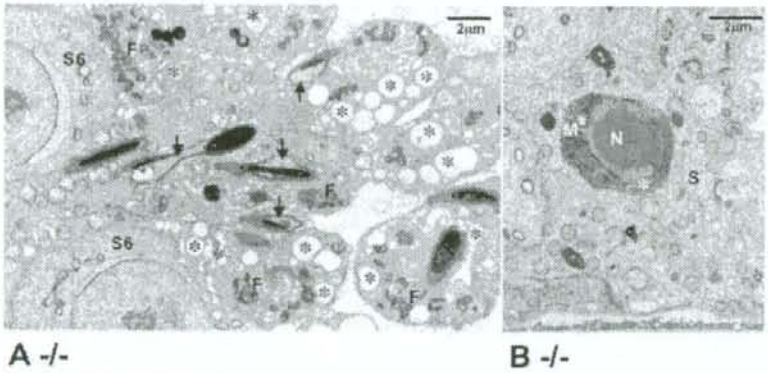

FIGURE 4. **Electron micrographs showing the degeneration of spermatids.** Sections of *MCA* homozygous mutant testis are shown. *A*, spermatids in a stage VI seminiferous tubule. Step 15 spermatids show deformation of the heads (*arrow*) and numerous vacuoles (*) in the cytoplasm. Flagella (*F*) that contain an axoneme, mitochondria, outer dense fibers, and fibrous sheaths are formed; however, these components are disarranged in the cytoplasm. Step 6 spermatids (*S6*) appear to be normal in shape. *B*, spermatid phagocytosed by Sertoli cells (*S*). The highly deformed nucleus/head (*N*), acrosome (*), and mitochondrial sheath (*M*) of the spermatids are shown.

mental Fig. S4). These findings indicate that the absence of *MCA* expression leads to abnormalities in spermatid formation, which in turn results in the abnormal morphogenesis of other components of the sperm. Alternatively, the MCA protein may affect various aspects of sperm morphogenesis directly.

MCA Was Strongly Associated with the ODF—Western blots of the subcellular fractions of sperm proteins indicated that MCA expression was present predominantly in the flagellum and more weakly in the sperm head (Fig. 5*A*). We also performed subcellular fractionation of sperm proteins located in the membrane/cytoplasm, axoneme, ODF, and FS/H. Soluble fractions and the final FS/H-insoluble fractions were separated by SDS-PAGE, transferred to a membrane, and subjected to Western blotting with anti-MCA antibody. MCA was weakly eluted in the membrane fraction that solubilized with a nonionic detergent (Triton X-100) but was mostly solubilized with potassium thiocyanate and urea (Fig. 5*B*). The majority of MCA was indeed recovered in the axoneme and ODF fraction, although a small amount of MCA remained in the nonextracted pellet that contained FS/H fractions (Fig. 5*B*). Izumo sperm-egg fusion 1 (Izumo1) (11) and AKAP82, the major protein of the fibrous sheath of the sperm flagellum (12), were present in the membrane and FS fractions, respectively. Odf1, the major ODF protein (13), was extracted only with urea (Fig. 5*B*). MCA was extracted together with the cytoskeletal elements that make up the axoneme, ODF, and FS.

To examine MCA-protein complexes, immunoprecipitation was performed. In immunoprecipitating complexes of testicular lysate with anti-Odf1, Odf2, and SHIPPO 1/Odf3, MCA co-precipitated with anti-Odf1 and Odf2 (Fig. 5*C*). Furthermore, we examined protein complexes with Septin 4 and Septin 7 (Fig. 5*C*) (22). No signals were detected in protein complexes with these annulus proteins. In addition,

Downloaded from www.jbc.org at OSAKA UNIVERSITY on January 18, 2009